NASA TECHNICAL MEMORANDUM

NASA TM X-2558

NASA TM X-2558

DYNAMICS OF A SUPERSONIC INLET-ENGINE COMBINATION SUBJECTED TO DISTURBANCES IN FUEL FLOW AND INLET OVERBOARD BYPASS AIRFLOW

by Robert E. Wallhagen, Francis J. Paulovich, and Lucille C. Geyser

Lewis Research Center
Cleveland, Ohio 44135

NATIONAL AERONAUTICS AND SPACE ADMINISTRATION • WASHINGTON, D. C. • MAY 1972

1. Report No.	2. Government Accession No.	3. Recipient's Catalog No.
NASA TM X-2558		

4. Title and Subtitle	5. Report Date
DYNAMICS OF A SUPERSONIC INLET-ENGINE COMBINATION SUBJECTED TO DISTURBANCES IN FUEL FLOW AND INLET OVERBOARD BYPASS AIRFLOW	May 1972
	6. Performing Organization Code
7. Author(s)	8. Performing Organization Report No.
Robert E. Wallhagen, Francis J. Paulovich, and Lucille C. Geyser	E-6115
	10. Work Unit No.
9. Performing Organization Name and Address	764-74
Lewis Research Center National Aeronautics and Space Administration Cleveland, Ohio 44135	11. Contract or Grant No.
	13. Type of Report and Period Covered
12. Sponsoring Agency Name and Address	Technical Memorandum
National Aeronautics and Space Administration Washington, D. C. 20546	14. Sponsoring Agency Code

15. Supplementary Notes

16. Abstract

An axisymmetric mixed-compression supersonic inlet and a single-spool turbojet engine were dynamically tested at Mach 2.5. The propulsion system was subjected to sweep-frequency sinusoidal disturbances of either inlet overboard bypass airflow or engine main fuel flow. The disturbances were at a logarithmic sweep rate of 1 decade per minute. Dynamic responses were taken of signals throughout the propulsion system. Selected signals were reduced relative to the prime propulsion system parameters. The experimental data are presented in Bode plots. Most of the plots are for a frequency range of 1.0 to 50 hertz.

17. Key Words (Suggested by Author(s))	18. Distribution Statement
Supersonic inlet dynamics; air breathing; engine dynamics; propulsion system dynamics; sweep frequency dynamic testing	Unclassified - unlimited

19. Security Classif. (of this report)	20. Security Classif. (of this page)	21. No. of Pages	22. Price*
Unclassified	Unclassified	46	$3.00

* For sale by the National Technical Information Service, Springfield, Virginia 22151

DYNAMICS OF A SUPERSONIC INLET-ENGINE COMBINATION SUBJECTED TO DISTURBANCES IN FUEL FLOW AND INLET OVERBOARD BYPASS AIRFLOW

by Robert E. Wallhagen, Francis J. Paulovich, and Lucille C. Geyser

Lewis Research Center

SUMMARY

An investigation has been made to determine experimentally the dynamic response of a supersonic mixed-compression inlet coupled to a single-spool turbojet. At the inlet design Mach number of 2.5, 60 percent of the supersonic area contraction occurred internally. Open-loop dynamic responses of selected signals throughout the inlet and engine were taken while the inlet was subjected to one of two different disturbances. Main engine fuel flow was disturbed at three engine operating points, and inlet overboard bypass airflow was symmetrically disturbed at one engine operating point. The disturbances were sinusoidal sweep frequencies at a logarithmic sweep rate of 1 decade per minute.

Frequency response analysis of the experimental data was accomplished using the sweep-frequency technique described in the report. The data reduction technique used analog and digital computation, with the final output as Bode plots. The final frequency response plots were calculated relative to the disturbance signals. Most of the presented Bode plots are over the frequency range from 1.0 to 50 hertz. Polar plots of selected signals are presented that include modeled responses from steady state to the 1-hertz frequency point.

INTRODUCTION

As flight requirements for supersonic aircraft increase beyond Mach 2, demands for increased performance and efficiency are placed on the propulsion system. A critical area in the search for increased performance and efficiency is the control of the normal shock position of the supersonic inlet. With the normal shock located immediately downstream of the aerodynamic throat (the position that generally results in maximum pres-

sure recovery and minimum distortion of the total pressure profile at the engine compressor face) the inlet is subject to unstart for the slightest disturbance tending to move the shock upstream. To insure against unstarts, the shock must be positioned sufficiently downstream of the aerodynamic throat so that large disturbances cannot move the shock in front of the throat. Through the use of active normal shock control, disturbances to the inlet can be counteracted before they affect the shock too severely. The faster a control can sense a disturbance and move to counteract it, the closer the normal shock can be located to the aerodynamic throat.

In order to design an active control for normal shock position, it is necessary to have an accurate dynamic model of the propulsion system. A good dynamic model has value for other facets of propulsion system engineering also. Computer simulations for studying interactions in high-performance multistage compressors can be improved with the use of experimental dynamic compressor data. Similarly, analytical work on combustor dynamics will benefit from high-frequency experimental propulsion system data. Then, of course, the engine main fuel control designer can use improved dynamic data to evaluate new or improved fuel control schemes.

Disturbances that affect a supersonic propulsion system can be classified in two categories: upstream and downstream. Upstream disturbances include changes in flight Mach number, angle of attack, capture air density, and gusts. Downstream disturbances are changes in overboard bypass airflow, inlet bleed airflow, engine combustor pressure, engine speed, and engine exhaust nozzle area.

Early jet engine dynamic studies are presented in references 1 to 3. References 1 and 2 used step disturbances in engine fuel flow and exhaust nozzle area. The engine dynamics were characterized by measurements of gain, time constants, and initial rise ratios. The dynamics study presented in reference 3 used high-frequency pressure transducers throughout the compressor and at the compressor and turbine discharge. The object of that study was to find indicators of surge and stall. Most of the disturbances used were steps in fuel flow to force the compressor discharge pressure past the surge limit. Reference 3 does, however, contain one frequency response plot of engine pressure signals for a sinusoidal disturbance in engine fuel flow. All these early studies were done at an inlet airflow velocity of Mach 0 to 0.88.

To further an understanding of dynamic interactions in a supersonic inlet-engine combination, a J85-13 turbojet engine with afterburner was run with a Lewis designed supersonic inlet. The tests were carried out at Mach 2.5 in the Lewis 10- by 10-Foot Supersonic Wind Tunnel. The tests were limited to downstream disturbances only because there were no practical means to generate upstream disturbances to frequencies approaching 50 hertz. The engine exhaust nozzle area was not disturbed, because with the engine turbine normally choked, little effect would be seen through the propulsion system. Also, the electrohydraulic actuator servo, used to position the exhaust nozzle,

would not permit disturbances at frequencies much above 10 hertz. The afterburner was not used, as it also would have been of little significance.

Frequency response data of various inlet-engine signals are presented for disturbances of engine main fuel flow and for disturbances of inlet overboard bypass airflow. Most of the data presented covers the frequency range from 1 to 50 hertz. Exceptions are engine rotor speed and turbine exit temperature, whose dynamics do not go that high in frequency, and a few other signals where the signal-to-noise ratio made the data meaningless.

The development of a generalized simulation for turbojet engines, which made use of the dynamic data in this report, is presented in reference 4. An analytical study on supersonic inlet dynamics, which used earlier but similar experimental dynamic data, is reported in reference 5. During the wind-tunnel program that obtained these dynamic data, an investigation was made into integrated inlet-engine control systems. The two reports resulting from the controls investigation (refs. 6 and 7) made use of closed-loop dynamic data that were obtained and reduced in the same manner as the open-loop dynamic data presented here.

SYMBOLS

A_{bpd}	area of bypass doors, cm^2
C	relative magnitude of signal response amplitude to disturbance amplitude
H	total pressure, N/cm^2
N	engine rotor speed, rad/sec
P	static pressure, N/cm^2
T	total temperature, K
t	time, sec
W	weight flow, kg/hr
X_{sp}	shock position motion, cm
ΔP_{fn}	pressure drop across fuel nozzles, N/cm^2
θ	angular displacement of sinusoidal disturbance input, deg

ψ	angular phase difference between disturbance and response, deg
Subscripts:	
fm	fuel manifold
fv	fuel valve
1,2,...,5	propulsion system station numbers
1.56(1.80, etc)	inlet station; 56 cm (80 cm, etc) downstream from cowl lip
2.1(2.2, etc)	compressor station at exit of first (second, etc) stage

TEST FACILITY AND APPARATUS

Model

A cut-away view of the inlet-engine combination is shown in figure 1. The inlet is a Lewis Research Center designed axisymmetric mixed-compression inlet, which at its design operating point has 60-percent of the supersonic area contraction occurring internally. The inlet has a cowl lip diameter of 0.473 meter, and its design corrected airflow at Mach 2.5 is 16.2 kilograms per second. There are boundary-layer bleeds provided in the throat region on both the centerbody and cowl surfaces. Six symmetrically spaced overboard bypass doors are provided at the diffuser exit to match inlet capture airflow to engine airflow. The centerbody translates for off-design conditions and for starting the inlet. The engine is a single spool turbojet with afterburner. The compressor has eight stages with variable angle guide vanes ahead of the first stage of the rotor and stability bleed ports at the exits of the third, fourth, and fifth stages. The engine uses an annular combustor with a two-stage turbine. A variable area exhaust nozzle is located downstream of the afterburner. A fuel selector valve was located upstream of the fuel spray nozzles; it allowed for fuel metering either by the normal hydromechanical fuel control of the engine or by a remotely located NASA-designed fuel valve. The fuel from the metering valve that was not connected to the engine was ported through an equivalent flow impedance back to the supply tank. Figure 2(a) gives a sketch of the overall fuel system. The other engine variables, compressor inlet guide vanes and the exhaust nozzle, were normally scheduled by the hydromechanical engine control, but could be manually controlled from the wind-tunnel control room. The inlet variables were manually adjusted from the control room. Detailed information on the inlet is available in references 8 and 9.

Disturbance Devices

Dynamic data were taken in response to two different types of disturbances. Both of these disturbances resulted in a change in net inlet airflow at the aft end of the inlet. Neglecting small amounts of boundary-layer bleed flow and ejector bypass flow, the net inlet airflow is equal to the sum of overboard bypass and engine airflow. The first type of disturbance was implemented by oscillating engine fuel flow with a high-response electrohydraulically actuated fuel valve. The second disturbance was accomplished by oscillating the overboard bypass doors with high-response electrohydraulic servos. Both devices were developed at Lewis. The disturbance in fuel flow caused a change in engine airflow by both changing engine mechanical speed and the compressor pressure ratio.

The high-speed fuel valve was driven by an electrohydraulic servo actuator. A sketch of the research fuel valve is shown in figure 2(b). Detailed information on the fuel valve can be obtained from reference 10. The position response of the fuel valve was flat within 0 to ±3 decibels for a frequency range of 0 to 110 hertz and for amplitudes yielding a 10-percent change (zero-to-peak) in fuel flow at the desired engine operating points. The engine operating points and the fuel flow levels are tabulated in table I.

TABLE I. - SUMMARY OF ENGINE OPERATING POINTS USED IN EXPERIMENTAL TESTS WITH FUEL-FLOW DISTURBANCES

Test number	Percent corrected speed	Compressor pressure ratio	Nominal fuel flow, kg/hr	Fuel disturbance (zero-to-peak), kg/hr	Fuel nozzle pressure drop (zero-to-peak), N/cm^2
1	87.8	4.17	272	27	2.2
2	83.0	3.77	390	41	3.0
3	88.2	4.63	490	50	4.4

A bypass door assembly is shown in figure 3. There were six of these assemblies, evenly spaced circumferentially around the inlet. The axial location of the bypass doors can be seen from figure 1. The bypass door response to a sinusoidal input was also flat to within 0 to ±3 decibels for a frequency range of 0 to 110 hertz and a door displacement of 0.2 centimeter, zero-to-peak. This displacement causes a zero-to-peak change in bypass airflow of 7.5 percent of maximum or approximately 1 kilogram per second. Further information about the bypass doors and the high response servo may be obtained from reference 11.

Although the object of oscillating the bypass doors and fuel valve was to obtain a direct change in inlet overboard bypass airflow and engine fuel flow; this was not completely accomplished. The overboard bypass doors of the inlet are choked with the inlet in normal started operation, so bypass airflow is directly a function of bypass door area and, hence, bypass door position. Since the fuel is an incompressible fluid, fuel flow at the metering valve is a direct function of fuel metering valve position, also. However, the fuel metering valve was located outside the 10- by 10-Foot Wind Tunnel and was connected to the engine fuel manifold by seven meters of tubing, some of which was heavy flex tubing. This allowed for dynamics in the fuel response at the spray nozzles, relative to that at the fuel valve. Thus, although fuel at the metering valve was a direct function of fuel valve position, the engine fuel flow at the fuel spray nozzles was not. This problem was alleviated by sensing fuel manifold pressure just upstream of the fuel nozzles and using it to indicate engine fuel flow instead of using the fuel metering valve position.

Instrumentation

A cross-sectional sketch of the inlet-engine combination without afterburner is shown in figure 4. All instrumentation points labeled with a P are static pressure taps. Points labeled with an H are total pressure taps. All pressure transducers are dynamic transducers of either the piezoelectric or strain gage type. The first subscripted number following a pressure transducer corresponds to the standard station numbers for an inlet and engine with a single spool. The numbers to the right of the decimal point in the subscripts further identify transducer locations between standard inlet-engine stations. In the inlet, the numbers to the right of the decimal point are axial distances, measured in centimeters, downstream from the inlet cowl lip. In the compressor, the number after the decimal point indicates the compressor stage where the transducer is located. The transducers were at the trailing edge of the compressor stators. Station 3.5 is a total pressure tap in the outer combustor cooling annulus. It is located approximately half way between stations 3 and 4. Turbine discharge temperature T_5 is the average of a rake of 18 chromel-alumel thermocouples. The fuel manifold pressure tap P_{fm} is located in one of the 12 spray nozzles. The signal X_{sp} is a stepwise continuous signal indicative of shock position. It is derived from the output of an electronic shock-position sensor, consisting of eight dynamic strain-gage pressure transducers. A detailed description of the shock-position sensor design and operation is available in reference 12. Both A_{bpd} and W_{fv} were outputs of LVDT's (linear variable differential transformers) located on the bypass doors and fuel valve metering spool, respectively. Although both of these outputs were position, simple scaling factors yielded area for the

bypass doors and fuel mass flow rate for the fuel valve. To account for changes in combustor pressure, the quantity $P_{fm} - H_{3.5}$ was formed and used as the difference in pressure across the fuel spray nozzles ΔP_{fn}.

All pressure transducers were mounted as close as practical to their respective ports to eliminate undesirable line dynamics. Most were located within 4 to 8 centimeters of the tap openings. A few were as much as 15 to 20 centimeters away.

Representative transducers were tested dynamically to 1000 hertz to check the effect of line dynamics. Figure 5 shows the frequency response (Bode) plots for representative transducers. As can be seen in figure 5 the transducer responses are reasonably flat to 100 hertz. The data that will be presented are cut off at 50 hertz, where the transducer error is less than 3 percent in the worst case and less than 2 percent for most signals. The phase error is 8^{o} or less at a frequency of 50 hertz.

Data Acquisition

Tests were run and data were taken for fuel-flow disturbances at three different engine operating points. The engine operating points are listed in table I. The engine was run up to the desired corrected speed on the manufacturers standard fuel control. It was then switched over to the NASA designed high-response fuel valve. To obtain data at off-design pressure ratios, the exhaust nozzle was manually opened or closed with fuel flow being adjusted to maintain the desired corrected speed. Fuel-flow disturbance test 1 was taken on the normal compressor operating line. Fuel-flow disturbance tests 2 and 3 were both taken above the normal operating line at a higher than design pressure ratio. For these two tests, the exhaust nozzle area was manually closed from its design setting. The zero-to-peak fuel-flow disturbance was chosen to be approximately 10-percent of the operating point fuel flow. The values of the operating point fuel flows and the disturbance amplitudes are also listed in table I.

Data were obtained for overboard-bypass-door disturbances at only one engine operating point. This engine operating point, on the normal operating line, was at a corrected speed of 86.4 percent and a pressure ratio of 4.13. The fuel flow was fixed at 360 kilograms per hour for this operating point. The nominal bypass-door area was 64 square centimeters. The zero-to-peak disturbance amplitude was approximately 25-percent of the nominal area.

The outputs of all transducers were recorded on two 14-channel magnetic tape recorders. A sweep-frequency oscillator was used as the input to the disturbance devices. With the sweep input to the bypass-door servo, the fuel valve servo command was held constant and vice versa. The sweep oscillator was set to a logarithmic sweep of 1 decade per minute over a frequency range from 0.5 to 140 hertz.

DATA REDUCTION TECHNIQUE

A schematic diagram of the basic data reduction technique is shown in figure 6. Both a sine wave and a cosine wave were available from the sweep oscillator, where the sine wave was used as the input to the disturbance device. Multiplying the transducer outputs by the sine and cosine outputs of the sweep oscillator and then filtering or averaging each of the products yields the real and imaginary parts of the signal dynamic response. By plotting these real and imaginary parts on the x and y axes, respectively, of an x-y plotter, a complete polar plot of the frequency response is obtained in a single input sweep. A detailed development of the equations involved in the sweep data reduction technique is available in reference 13.

The schematic diagram in figure 6 shows the ideal case where the sweep oscillator generates perfect sine and cosine signals of equal amplitude. In the actual case the sine and cosine outputs are not of equal amplitude, and the phase difference is not always 90°. Errors due to the imperfect sine and cosine signals are discussed in reference 13, and a method to correct the errors is presented therein.

Although the data can be reduced and corrected using an analog computer, there are significant advantages to using an analog computer for the multiplication and averaging and a digital computer for corrections and scaling. The chief advantage is that the final digital results can be stored on punched cards, facilitating the calculation of relative responses of data signals to other signals not originally on the same magnetic data tape. A second advantage is that calibration and scaling factors are easily incorporated and the data correction algebra is simpler to perform digitally. Also, converting the real and imaginary parts of the signal responses, to magnitude and phase data is easily done digitally.

The data presented in this report were reduced using both an analog and digital computer. The multiplication and filtering to obtain the real and imaginary parts of the responses and to obtain the correction factors, as described in reference 13, was done on an analog computer. The input to the analog computer came from the magnetic tape recorded from the experimental test. The sine and cosine signals from the sweep oscillator were also recorded on the magnetic tape during the running of the tests.

The outputs from the analog computer, real and imaginary parts of all the signals plus their correction factors, were recorded on another magnetic tape recorder. To obtain final plots of magnitude and phase as a function of frequency, a signal equal to the period of the disturbance signal was generated on the analog computer and recorded on magnetic tape. The analog computer output tape was then played back as the input to a 16-channel 16-bit digitizer with the digitized data being recorded on digital magnetic tape. The digital tape was then used as the input to a digital computer along with calibration and gain figures that had been prepunched on computer cards. The computer

calculated magnitude and phase data for all signals as a function of frequency and punched the results on cards.

After all the desired data had been processed through to computer output cards, selected blocks of cards could be reprocessed on the digital computer to generate relative frequency response plots. The output from this second computer run was a digital magnetic tape capable of driving a tape-controlled digital plotter. The output of the plotter was Bode plots, which are magnitude and phase plots, both as functions of frequency.

PRESENTATION OF DATA

Plot Description

Most of the data presented are shown plotted to 50 hertz. There are a number of reasons for cutting the traces off at this point. The primary reason is that at 50 hertz most signal levels have decreased to the background noise level of the data reduction process. Presenting data beyond 50 hertz would generally be meaningless or confusing. This problem is compounded by the process of calculating the response of a signal relative to its disturbance signal. In calculating the response of a good clean signal to a poor noisy signal, the good signal data are obscured by the noisy one. Another reason to stop the plotting at 50 hertz is to eliminate erroneous 60-hertz noise on a few of the experimental signals. A few traces have been stopped below 50 hertz because either the response signal or the disturbance signal was poor, even to 50 hertz.

All the magnitude frequency response plots have been normalized to unity at 1 hertz. The scaling factor or gain at this frequency is included on the plot. All these 1-hertz open-loop gains are also tabulated in table II for fuel-flow disturbances and in table III for bypass-door disturbances. The steady-state or zero-frequency gains are also included in tables II and III. Dynamic data are not available for the engine signals $P_{2.4}$ and $P_{2.5}$ because both of these transducers failed early in the experimental test. The steady-state data are taken with a separate steady-state pressure acquisition system.

The negative gain terms in tables II and III, indicate that the particular signal decreases for an increase in the disturbance signal. For the fuel-flow disturbance case an increase in fuel flow causes engine speed and compressor discharge pressure to increase. However, the increase in speed causes an increase in engine airflow, which causes a decrease in the inlet and compressor face pressure. Thus, inlet pressures and forward compressor stage pressures decrease for increasing fuel flow and compressor discharge pressure. For the bypass-door disturbance case an increase in overboard bypass airflow causes a decrease in all the pressures throughout the inlet and engine. Engine speed is the only signal that increases with increasing bypass-door area.

TABLE II. - SUMMARY OF OPEN LOOP, ZERO-TO-PEAK GAINS FOR FUEL FLOW DISTURBANCES

Signal	Units	Figure part	Test 1 (fig. 7)		Test 2 (fig. 8)		Test 3 (fig. 9)	
			Steady-state gain	1-Hz gain	Steady-state gain	1-Hz gain	Steady-state gain	1-Hz gain
P_{fm}/W_{fv}	$(N/cm^2)/(kg/hr)$	(a)	------	0.093	------	0.10	------	0.12
H_3/W_{fv}	$(N/cm^2)/(kg/hr)$	(b)	------	0.014	------	0.015	------	0.014
$H_{3.5}/P_{fm}$	Dimensionless	(c)	0.34	0.17	0.31	0.16	0.27	0.15
$H_5/\Delta P_{fn}$		(d)	0.14	0.07	0.17	0.050	0.13	0.040
$H_3/\Delta P_{fn}$		(e)	0.48	0.19	0.47	0.17	0.38	0.14
$H_2/\Delta P_{fn}$		(f)	-0.080	0.030	-0.07	0.020	-0.05	0.020
$P_2/\Delta P_{fn}$		(g)	-0.080	0.030	-0.06	0.020	-0.05	0.020
$P_{1.93}/\Delta P_{fn}$		(h)	-0.10	0.030	-0.09	0.010	-0.07	0.020
$P_{1.56}/\Delta P_{fn}$		(i)	-0.43	0.11	-0.29	0.11	-0.20	0.070
$N/\Delta P_{fn}$	$(rad/sec)/(N/cm^2)$	(j)	9.7	3.0	9.0	2.4	7.0	2.3
$T_5/\Delta P_{fn}$	$K/(N/cm^2)$	(k)	14	1.5	19	2.0	13	1.7
$P_{2.7}/H_3$	Dimensionless	(l)	0.66	0.56	0.69	0.64	0.68	0.71
$P_{2.6}/H_3$		(m)	0.47	0.26	0.50	0.38	0.48	0.37
$P_{2.5}/H_3$		---	0.32	-----	0.32	-----	0.30	-----
$P_{2.4}/H_3$		---	0.20	-----	0.16	-----	0.19	-----
$P_{2.3}/H_3$		(n)	0.050	0.060	0.060	0.07	0.080	0.010
$P_{2.2}/H_3$		(o)	-0.040	0.13	0.010	0.11	0.010	0.16
$P_{2.1}/H_3$		(p)	-0.11	0.18	-0.070	0.15	-0.050	0.19
P_2H_3		(q)	-0.16	0.16	-0.13	0.13	-0.14	0.16
$P_{1.93}/H_3$		(r)	-0.21	0.15	-0.20	0.12	-0.19	0.17
$P_{1.80}/H_3$		(s)	-0.22	0.16	-0.22	0.15	-0.22	0.17
$P_{1.56}/H_3$		(t)	-0.89	0.62	-0.65	0.65	-0.52	0.51
N/H_3	$(rad/sec)/(N/cm^2)$	(u)	20	16	20	14	18	16

TABLE III. - SUMMARY OF OPEN LOOP ZERO-TO-PEAK GAINS FOR BYPASS-DOOR DISTURBANCES

[Engine operating corrected speed, 86.4 percent; pressure ratio, 4.13.]

Signal	Units	Part of fig. 10	Steady-state gain	1-Hz gain
X_{sp}/A_{bpd}	cm/cm^2	(a)	-------	0.11
$P_{1.56}/A_{bpd}$	$(N/cm^2)/cm^2$	(b)	-0.051	0.016
$P_{1.93}/A_{bpd}$	↓	(c)	-0.011	0.0032
P_2/A_{bpd}	↓	(d)	-0.0070	0.0032
H_2/A_{bpd}	↓	(e)	-0.0062	0.0041
H_3/A_{bpd}	↓	(f)	-0.019	0.040
N/A_{bpd}	$(rad/sec)/cm^2$	(g)	0.18	0.030
$P_{2.1}/P_2$	Dimensionless	(h)	1.2	1.2
$P_{2.2}/P_2$	↓	(i)	1.4	1.4
$P_{2.3}/P_2$	↓	(j)	1.8	2.1
$P_{2.4}/P_2$	↓		2.3	
$P_{2.5}/P_2$	↓		2.5	
$P_{2.6}/P_2$	↓	(k)	2.7	3.0
$P_{2.7}/P_2$	↓	(ℓ)	2.6	3.1
H_3/P_2	↓	(m)	2.7	3.5
$H_{3.5}/P_2$	↓	(n)	2.8	3.4
H_5/P_2	↓	(o)	0.98	1.1
$X_{sp}/P_{1.93}$	$cm/(N/cm^2)$	(p)	-------	31
$P_{1.56}/P_{1.93}$	Dimensionless	(q)	4.5	5.0
$P_{1.80}/P_{1.93}$	↓	(r)	0.95	1.4
$P_2/P_{1.93}$	↓	(s)	0.62	1.0
$X_{sp}/P_{1.56}$	$cm/(N/cm^2)$	(t)	-------	6.3

This is because, for a fixed fuel flow, engine speed increases for a reduced compressor face pressure.

For fuel-flow disturbances the most important engine parameters and selected inlet parameters (which are normally used to monitor and control the propulsion system) were referenced to two primary signals. One signal was the pressure drop across the fuel nozzle ΔP_{fn}, which gave the best indication of disturbance fuel flow. The pressure drop was computed as the difference between fuel manifold pressure P_{fm} and combustor total pressure $H_{3.5}$. The zero frequency change in ΔP_{fn}, which corresponds to the 10-percent change in fuel flow, is listed in table I. The second signal used as a reference for the fuel-flow disturbance data was compressor discharge total pressure H_3. All dynamic signals through the compressor and inlet are plotted relative to H_3. Engine speed N is included in this last group of plots to indicate how the inlet and first few compressor stages follow engine speed at low frequency. Also used as reference signals in the data reduction process are the fuel metering valve mass flow W_{fv} and the fuel manifold pressure P_{fm}. The plots P_{fm}/W_{fv} and H_3/W_{fv} are presented to show the fuel line dynamics that were present in the experimental test setup. Because of these fuel line dynamics, the fuel metering valve position could not be used as a reference for the important propulsion parameters. The plot of $H_{3.5}/P_{fm}$ is presented to show the relation of combustor total pressure $H_{3.5}$ to fuel manifold pressure.

The fuel-flow disturbance data plots are presented in the order, listed in table II. Plots for tests 1 to 3 are presented in figures 7 to 9.

Bypass-Door Disturbance Data

For the tests where overboard-bypass doors were the disturbance device, the area of the bypass doors A_{bpd} was the prime variable that other signals were referenced to. All the engine pressure transducers were also referenced to compressor-face static pressure P_2. Compressor-face static pressure was used rather than the total-pressure signal, because it contained the same dynamic pressure signal but had less high-frequency inlet noise superimposed on it. All the inlet static-pressure signals were also referenced to $P_{1.93}$, which was the inlet static pressure immediately upstream of the bypass-door cavity. The shock position signal X_{sp}, referenced to throat exit static pressure $P_{1.56}$, is included so show how the shock position and $P_{1.56}$ are related. Throat exit static pressure is a signal commonly used to indicate shock position for normal shock controllers.

The bypass-door disturbance plots are presented in the order that they are listed in table III. The plots are shown in figure 10.

Composite Plot

To show how the pressures vary through the compressor and inlet for fuel-flow disturbances, a composite plot is shown in figure 11. All signals are for fuel-flow disturbance test 1 and are plotted relative to compressor discharge total pressure H_3. Clearly evident from figure 11(a) is that the rear compressor pressure signals follow H_3 very closely. The effect of H_3 extends as far forward as the output of compressor stage 3, $P_{2.3}$. The forward compressor signals and all the inlet signals follow engine speed, which is also plotted. Figure 11(b) shows that the phase of engine speed and that of the various inlet and forward compressor signals are 180° apart. As explained earlier, as engine rotor speed increases, engine airflow increases, which draws the inlet normal shock downstream causing lower inlet and compressor face pressures.

At low frequency, compressor station $P_{2.3}$ is nearest to the point where the reducing effect of engine speed and the increasing effect of H_3 cancel. This is seen in table II by the very low gain of $P_{2.3}/H_3$. As the frequency of the disturbance is increased, the effect of fuel flow oscillations on engine speed attenuates more rapidly than its effect on compressor discharge pressure. This causes a slight shift in the cancellation point. This small shift appears to have a dramatic effect on the frequency response of $P_{2.3}/H_3$, which is especially evident for fuel-flow disturbance test 3 (see fig. 9(n)). The $P_{2.3}/H_3$ plot for test 3 has a much greater gain increase than for test 1 or 2 because the 1-hertz gain is much lower.

A composite plot of compressor signals, subjected to inlet overboard-bypass-door airflow disturbances, is not presented as it would not contain interesting dynamics. The reason for the lack of interesting dynamics in the compressor signals is that the engine speed response for the bypass-door airflow disturbance is only one tenth of that for the fuel-flow disturbance. Thus, the effect of speed on the compressor pressure signals is barely evident, and there is no indication of a phase reversal through the compressor.

MODELED DYNAMICS BELOW ONE HERTZ

A comparison of the steady-state and 1-hertz gain terms in tables II and III indicates that significant dynamic changes occur between steady-state and a frequency of 1 hertz. In order to present a full picture of the dynamics involved, a simple modeling scheme was used to depict the complete response of a few selected signals.

The response of pressure signals throughout the propulsion system to a disturbance in engine fuel flow can be separated into two parts. The first part is the effect of a change in combustor pressure due to the fuel disturbance, and the second part is the effect that relates to the engine speed change. The effect of changes in engine speed is

much greater than that of changes in combustor pressure; however, the effect of speed decreases rapidly with frequency. Table II indicates that at 1 hertz the engine speed response is 1/3 of its zero-frequency response. The attenuation in the engine speed response is due to the engine rotor inertia and can be modeled quite accurately by a simple first-order lag. On a polar plot a first-order lag appears as a semicircle, starting at the steady-state gain with zero-degree lag and going to zero gain (the origin) asymptotically with the 90° lag axis. The experimental dynamic speed data referenced to ΔP_{fn} from test 1 is plotted as a solid line on a polar plot in figure 12(a). The modeled first-order lag response from zero frequency to the 1-hertz point is added as a dashed line. It is apparent that the experimental data fits the first-order lag assumption well. For the rest of the signals it is assumed that the response below a frequency of 1.0 hertz is completely dominated by the speed effect. Thus, on a polar plot, the modeled response appears as a semicircle connecting the zero-frequency (steady state) gain point and the 1-hertz gain point. The experimental response on all plots appears as a solid line. Plots of T_5, H_5, H_3, H_2, and $P_{1.56}$ all referenced to ΔP_{fn} appear in figure 12.

By extrapolating the experimental speed plots below the 1-hertz frequency point, until they intersect the steady-state gain line, a break frequency of 0.3 hertz is determined. This point corresponds to the 45° lag point on the polar plot of speed, and is so labeled.

CONCLUSIONS

An axisymmetric mixed-compression supersonic inlet and a single-spool turbojet engine were dynamically tested at Mach 2.5. The propulsion system was subjected to sweep-frequency sinusoidal disturbances of inlet overboard bypass airflow or engine main fuel flow at a logarithmic sweep rate of 1 decade per minute. Open-loop frequency responses were taken of signals throughout the propulsion system. Selected signals were reduced relative to the prime propulsion system parameters. The following results were obtained:

(1) Open-loop magnitude and phase plots as a function of frequency were obtained of selected propulsion system signals for a frequency range of 1.0 to 50 hertz for fuel flow or inlet airflow disturbances.

(2) There is a phase reversal of pressure signals towards the front of the compressor in response to a fuel-flow disturbance.

(3) The low-frequency response (below 1.0 Hz) can be modeled without difficulty by assuming that the engine speed response is a first-order lag and that its effect predominates below 1.0 hertz.

(4) Frequency response analysis of experimental data can be accomplished through

the use of the sweep-frequency technique described. Final output of accurate Bode plots are possible with the option of later cross plotting selected signals.

This propulsion-system dynamic study is not complete in that disturbances to the engine variable geometry, engine exhaust nozzle, and engine afterburner were not implemented. Also disturbances upstream of the inlet were not tried. These disturbances were not used because it was felt either that they were of much less significance, in the case of the just mentioned engine variables, or that there was no means to implement them, in the case of the upstream inlet disturbances.

Lewis Research Center,
National Aeronautics and Space Administration,
Cleveland, Ohio, February 24, 1972,
764-74.

REFERENCES

1. Delio, Gene J.; and Rosenzweig, Solomon: Dynamic Response at Atltitude of a Turbojet Engine with Variable Area Exhaust Nozzle. NACA RM E51K19, 1952.
2. Craig, R. T.; Vasu, George; and Schmidt, R. D.: Dynamic Characteristics of a Single-Spool Turbojet Engine. NACA RM E53C17, 1953.
3. Delio, G. J.; and Stiglic, P. M.: Experimental Investigation of Control Signals and the Nature of Stall and Surge Behavior in a Turbojet Engine. NACA RM E54I15, 1954.
4. Seldner, Kurt; Mihaloew, James R.; and Blaha, Ronald J.: Generalized Simulation Technique for Turbojet Engine System Analysis. NASA TN D-6610, 1971.
5. Willoh, Ross G.: A Mathematical Analysis of Supersonic Inlet Dynamics. NASA TN D-4969, 1968.
6. Cole, Gary L.; Neiner, George H.; and Wallhagen, Robert E.: Coupled Supersonic Inlet-Engine Control Using Overboard Bypass Doors and Engine Speed to Control Normal Shock Position. NASA TN D-6019, 1970.
7. Paulovich, Francis J.; Neiner, George H.; and Hagedorn, Ralph E.: A Supersonic Inlet-Engine Control Using Engine Speed as a Primary Variable for Controlling Normal Shock Position. NASA TN D-6021, 1971.
8. Cubbison, Robert W.; Meleason, Edward T.; and Johnson, David F.: Performance Characteristics from Mach 2.58 to 1.98 of an Axisymmetric Mixed-Compression Inlet System with 60-Percent Internal Contraction. NASA TM X-1739, 1969.

9. Wasserbauer, Joseph F.: Dynamic Response of a Mach 2.5 Axisymmetric Inlet with Engine or Cold Pipe and Utilizing 60 Percent Supersonic Internal Area Contraction. NASA TN D-5338, 1969.

10. Batterton, Peter G.; and Zeller, John R.: Dynamic Performance Analysis of a Fuel-Control Valve for Use in Airbreathing Engine Research. NASA TN D-5331, 1969.

11. Neiner, George H.: Servosystem-Design of a High-Response Slotted-Plate Overboard Bypass Valve for a Supersonic Inlet. NASA TN D-6081, 1970.

12. Cole, Gary L.; Neiner, George H.; and Crosby, Michael J.: Design and Performance of a Digital Electronic Normal Shock Position Sensor for Mixed-Compression Inlets. NASA TN D-5606, 1969.

13. Drain, Daniel I.; Bruton, William M.; and Paulovich, Francis J.: Airbreathing Propulsion System Testing Using Sweep Frequency Techniques. NASA TN D-5485, 1969.

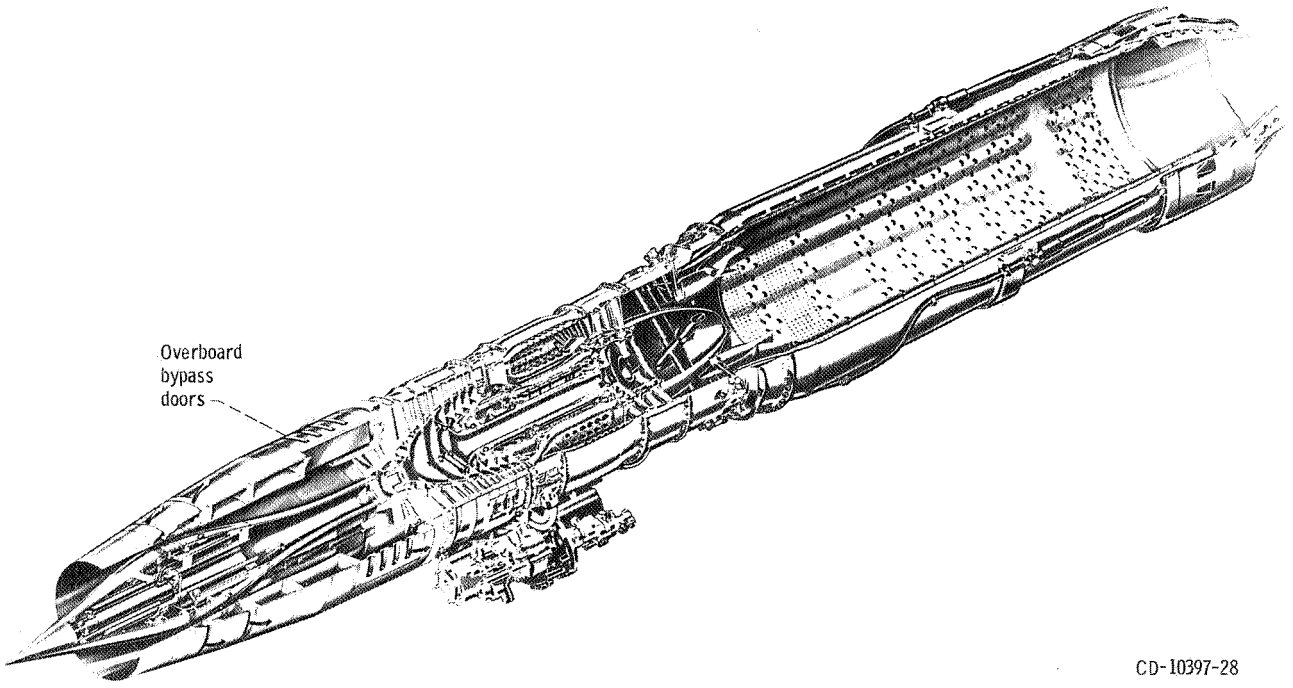

Figure 1. - Cut-away view of inlet-engine combination.

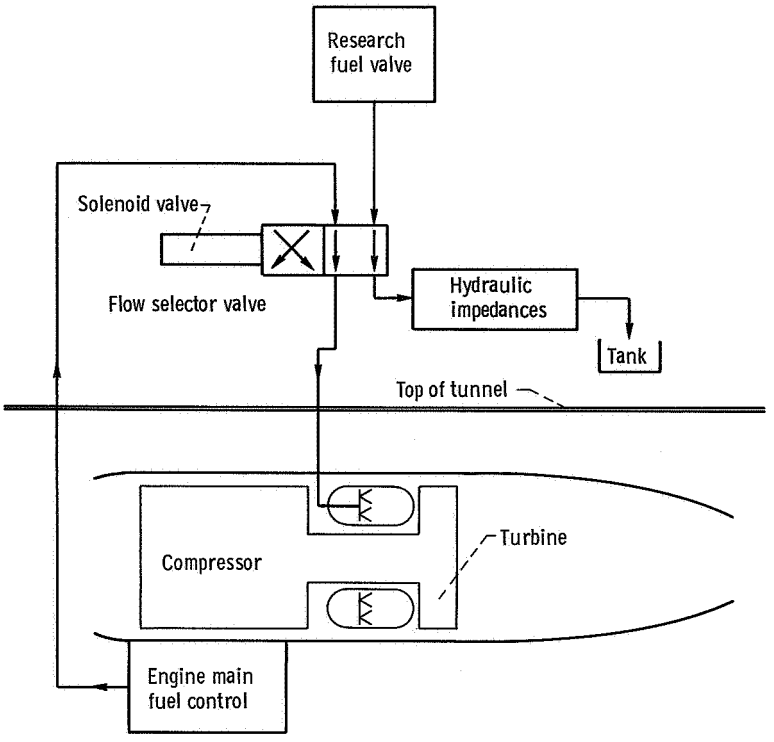

(a) Overall fuel system.

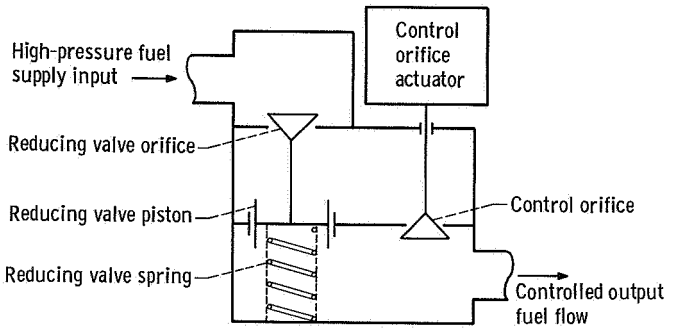

(b) Research fuel valve details.

Figure 2. - Engine hybrid fuel system.

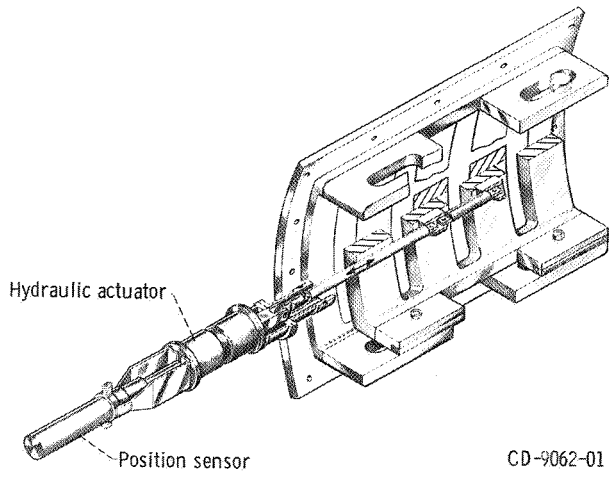

Figure 3. - Overboard-bypass-door assembly and actuator.

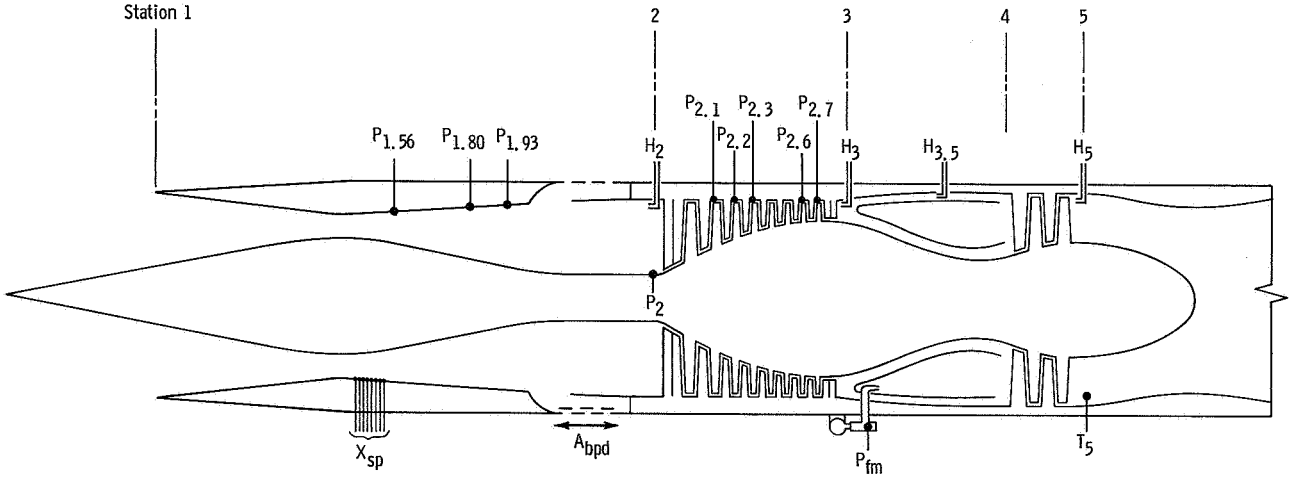

Figure 4. - Inlet-engine instrumentation layout.

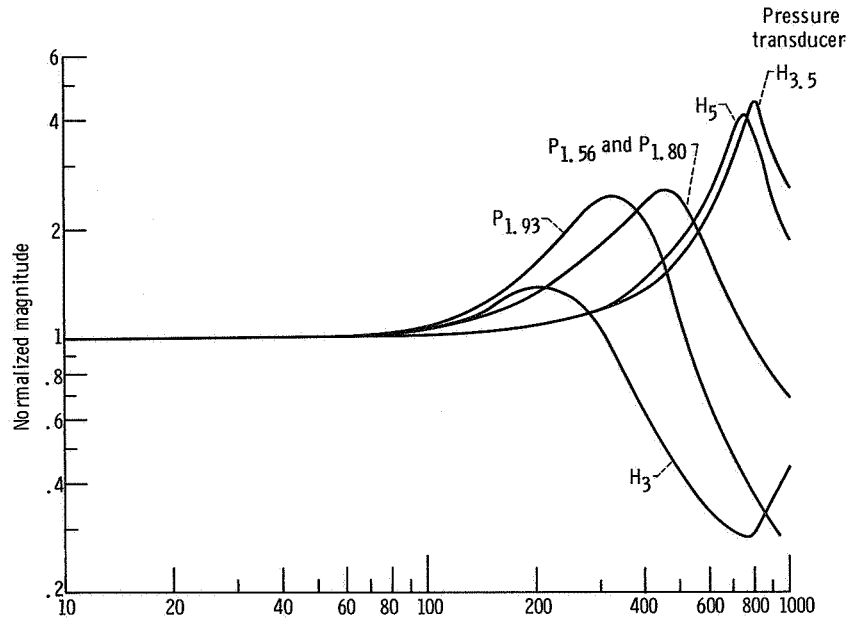

(a) Normalized amplitude response.

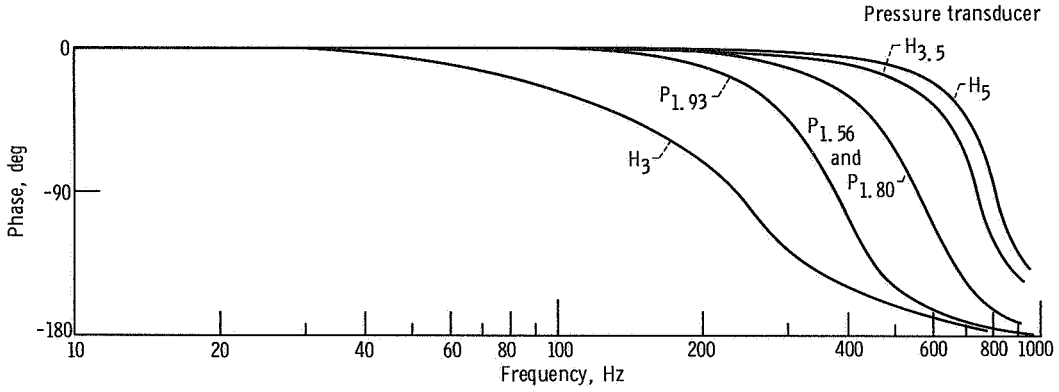

(b) Phase response.

Figure 5. - Frequency response of selected dynamic transducers.

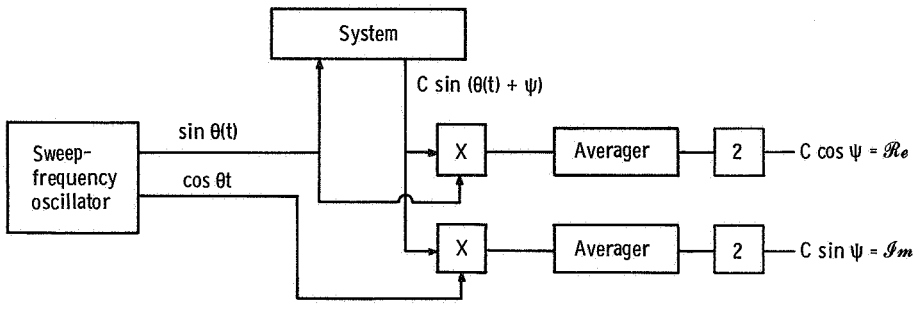

Figure 6. - Data reduction system.

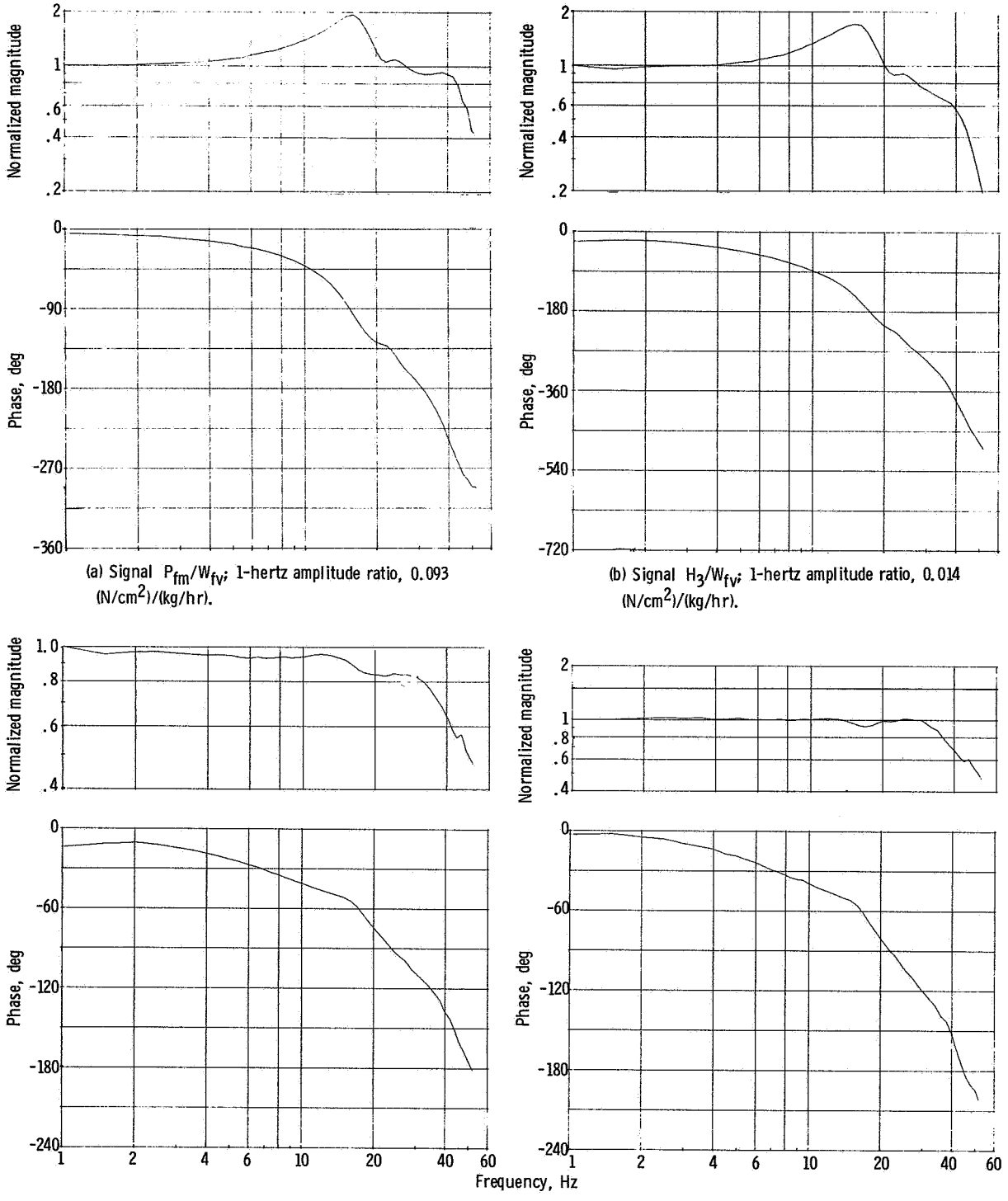

(a) Signal P_{fm}/W_{fv}; 1-hertz amplitude ratio, 0.093 $(N/cm^2)/(kg/hr)$.

(b) Signal H_3/W_{fv}; 1-hertz amplitude ratio, 0.014 $(N/cm^2)/(kg/hr)$.

(c) Signal $H_{3.5}/P_{fm}$; 1-hertz amplitude ratio, 0.17.

(d) Signal $H_5/\Delta P_{fn}$; 1-hertz amplitude ratio, 0.07.

Figure 7. - Normalized frequency responses of inlet and engine signals for fuel flow disturbances. Engine operating corrected speed, 87.8 percent; compressor pressure ratio, 4.17.

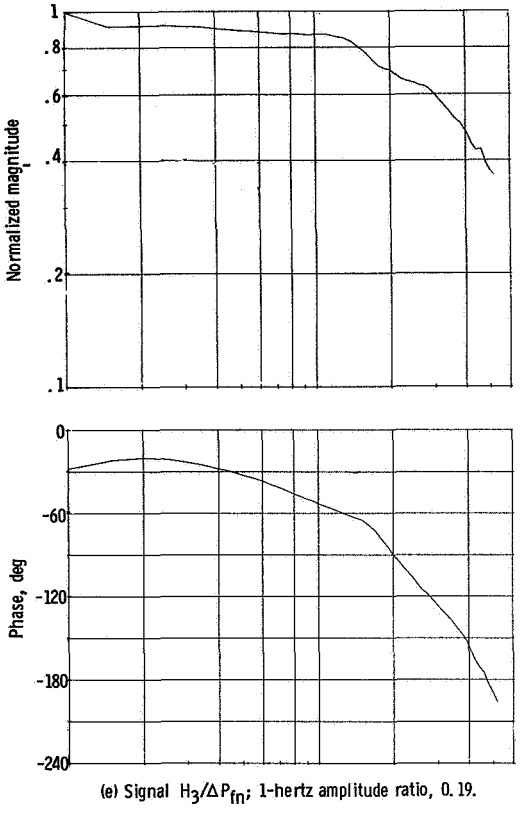

(e) Signal $H_3/\Delta P_{fn}$; 1-hertz amplitude ratio, 0.19.

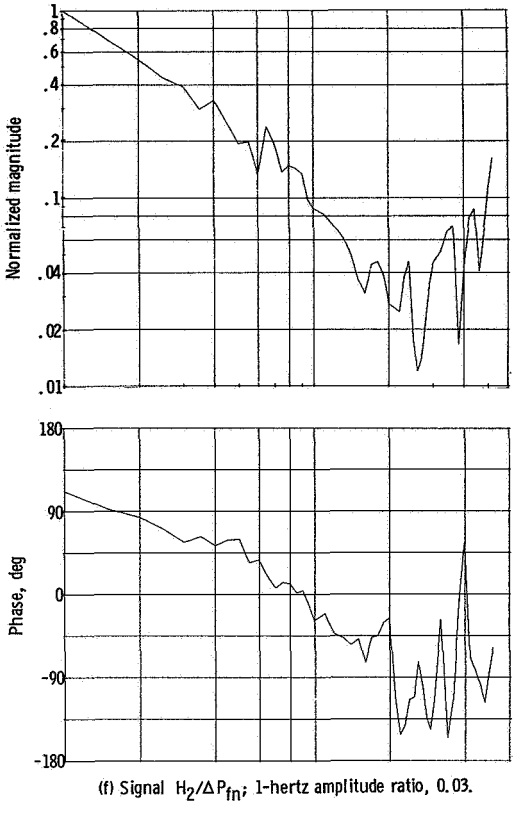

(f) Signal $H_2/\Delta P_{fn}$; 1-hertz amplitude ratio, 0.03.

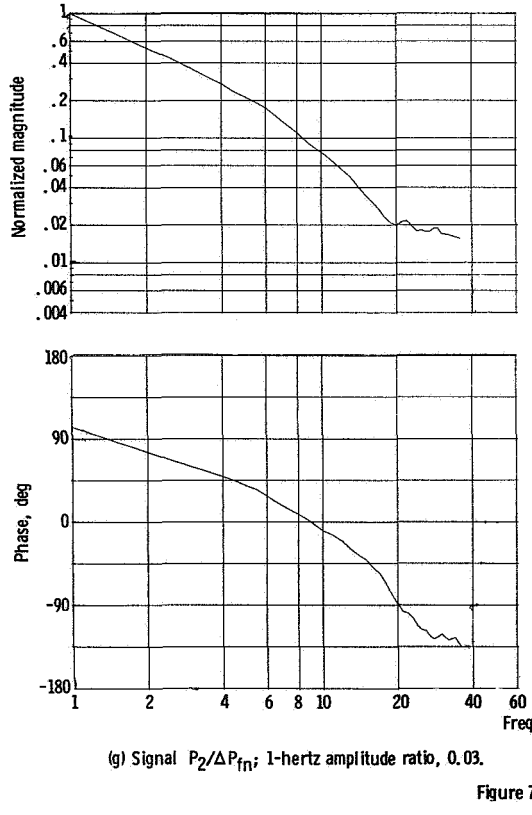

(g) Signal $P_2/\Delta P_{fn}$; 1-hertz amplitude ratio, 0.03.

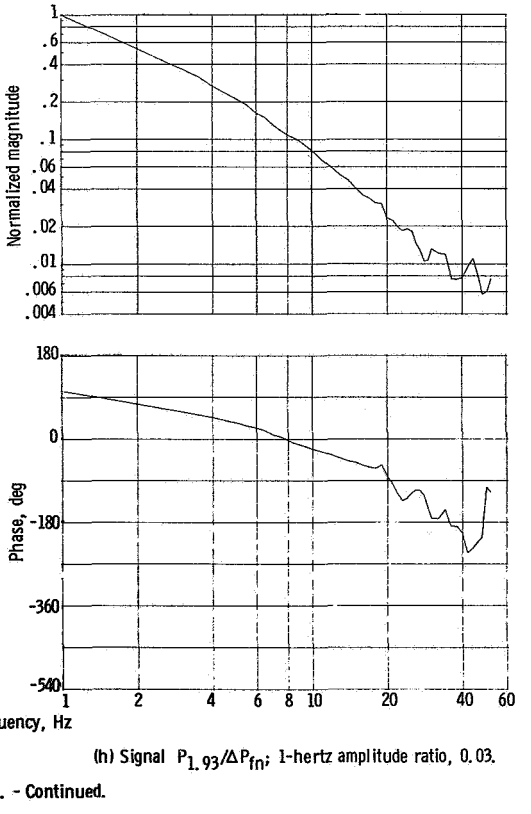

(h) Signal $P_{1.93}/\Delta P_{fn}$; 1-hertz amplitude ratio, 0.03.

Figure 7. - Continued.

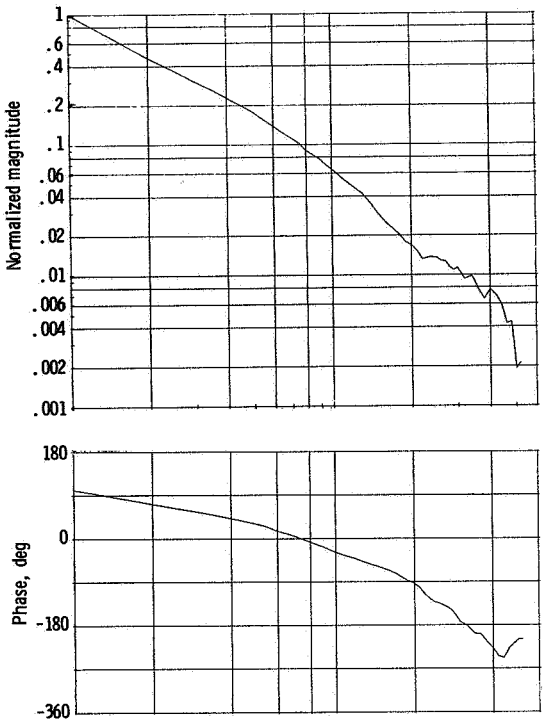

(i) Signal $P_{1.56}/\Delta P_{fn}$; 1-hertz amplitude ratio, 0.11.

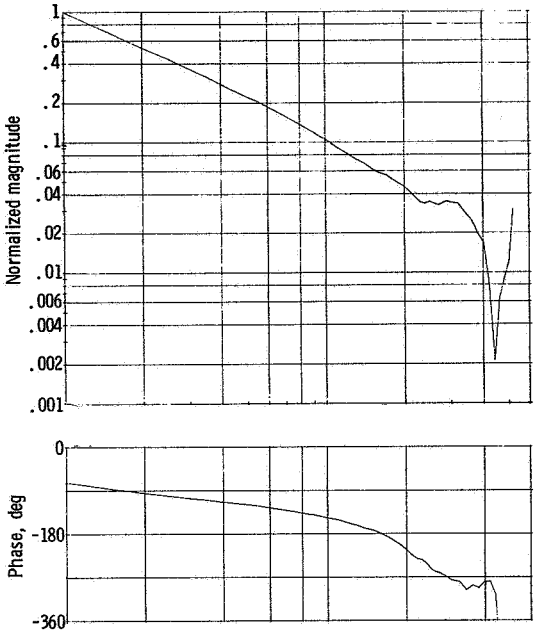

(j) Signal $N/\Delta P_{fn}$; 1-hertz amplitude ratio, 3 (rad/sec)/(N/cm^2).

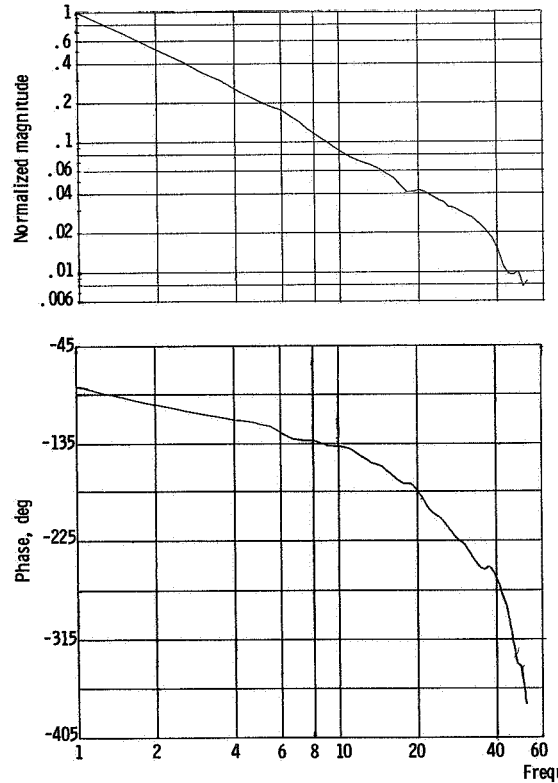

(k) Signal $T_5/\Delta P_{fn}$; 1-hertz amplitude ratio, 1.5 K/(N/cm^2).

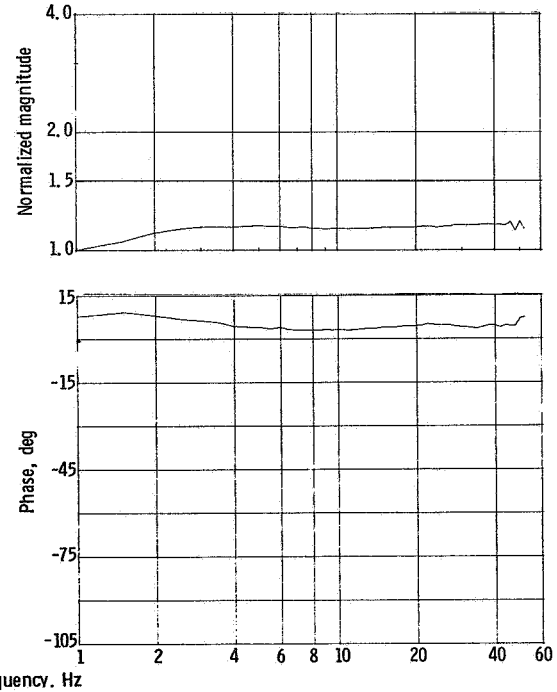

(ℓ) Signal $P_{2.7}/H_3$; 1-hertz amplitude ratio, 0.56.

Figure 7. - Continued.

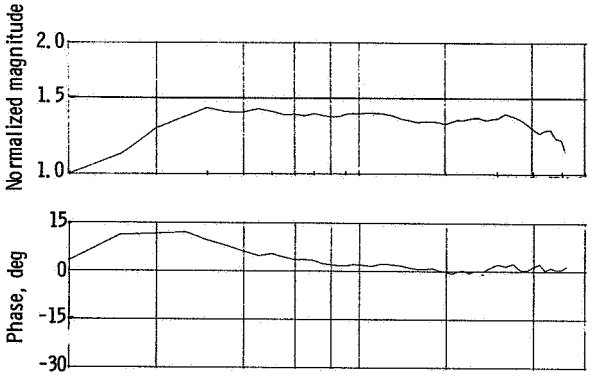

(m) Signal $P_{2.6}/H_3$; 1-hertz amplitude ratio, 0.26.

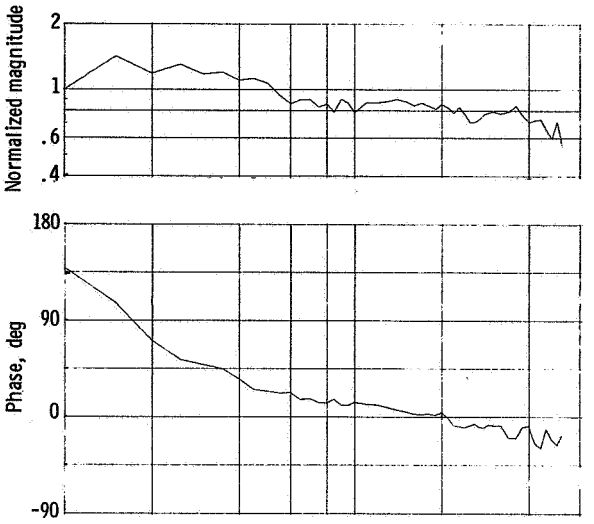

(n) Signal $P_{2.3}/H_3$; 1-hertz amplitude ratio, 0.06.

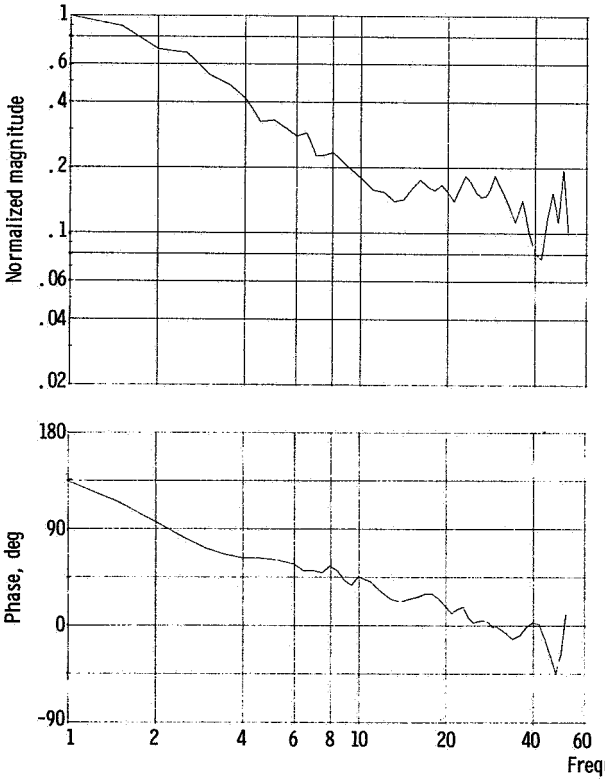

(o) Signal $P_{2.2}/H_3$; 1-hertz amplitude ratio, 0.13.

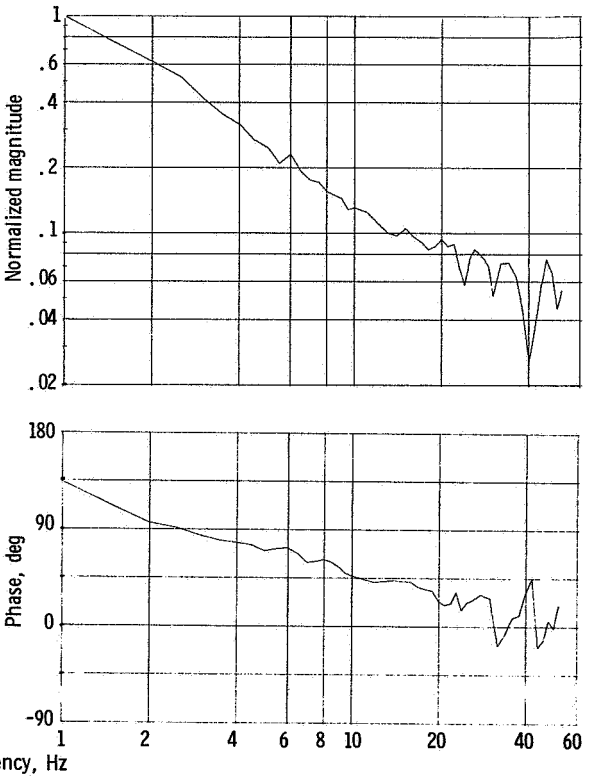

(p) Signal $P_{2.1}/H_3$; 1-hertz amplitude ratio, 0.18.

Figure 7. - Continued.

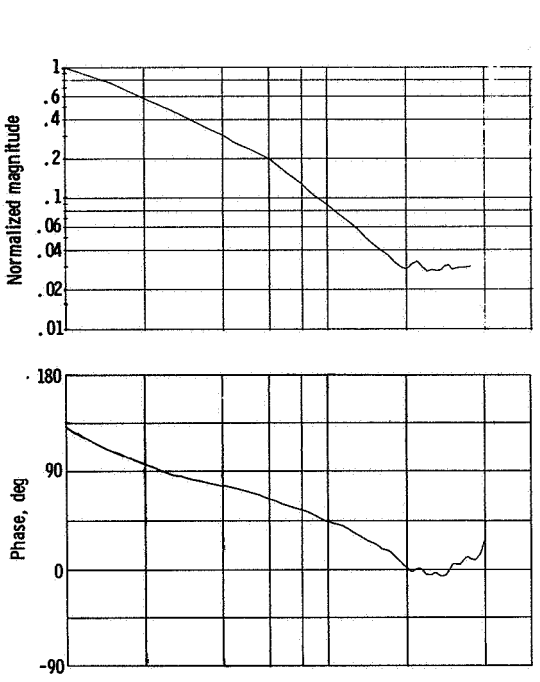

(q) Signal P_2/H_3; 1-hertz amplitude ratio, 0.16.

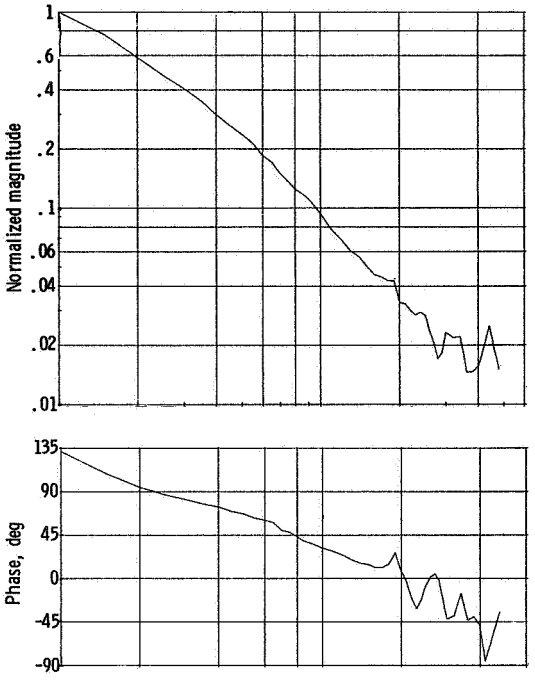

(r) Signal $P_{1.93}/H_3$; 1-hertz amplitude ratio, 0.15.

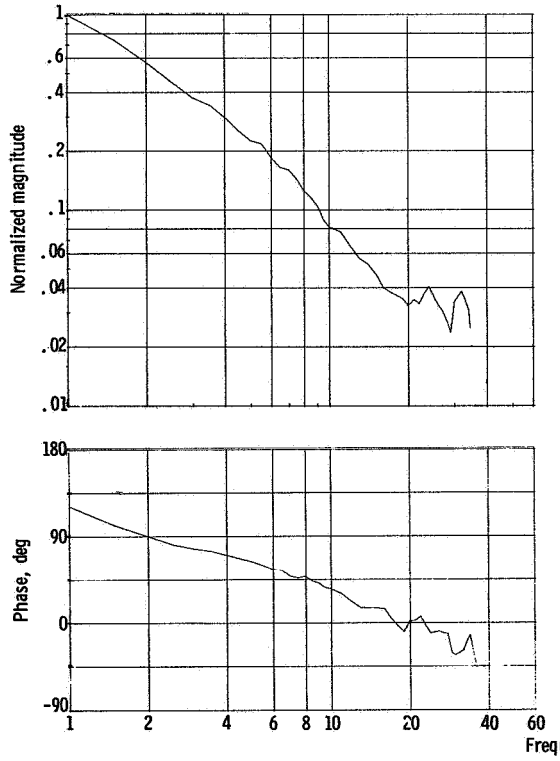

(s) Signal $P_{1.80}/H_3$; 1-hertz amplitude ratio, 0.16.

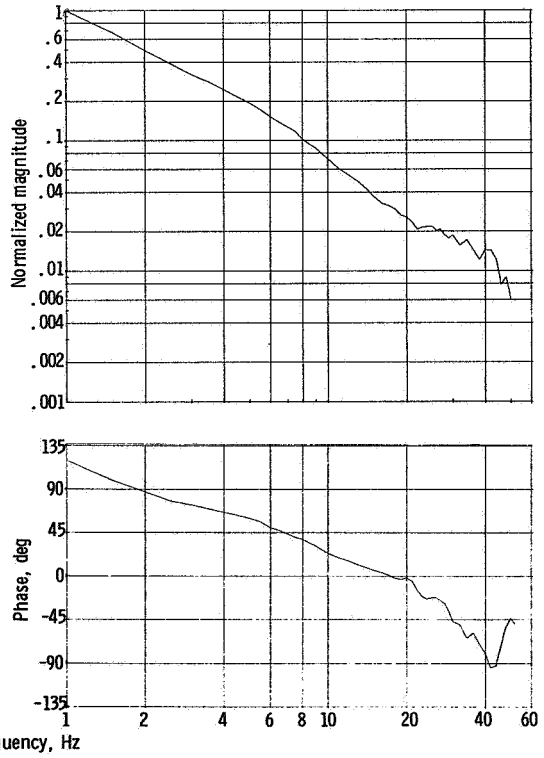

(t) Signal $P_{1.56}/H_3$; 1-hertz amplitude ratio, 0.62.

Figure 7. - Continued.

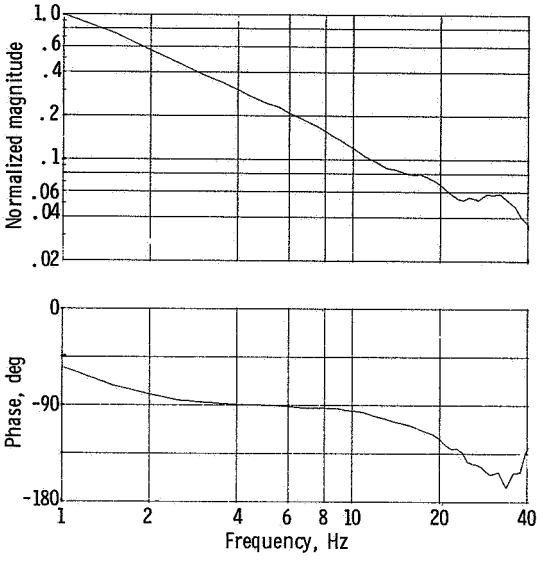

(u) Signal N/H_3; 1-hertz amplitude ratio, 16 (rad/sec)/(N/cm^2).

Figure 7. - Concluded.

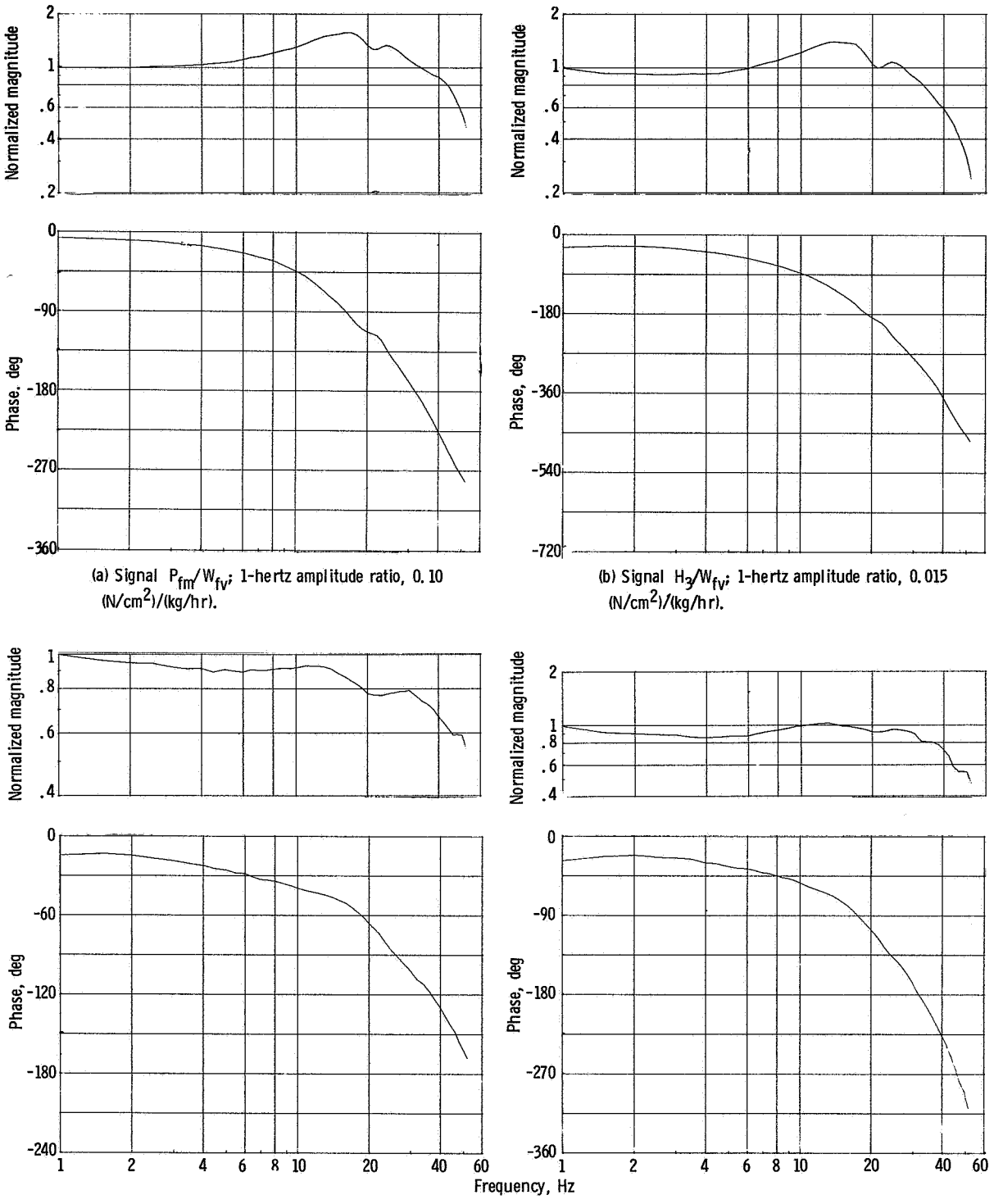

(a) Signal P_{fm}/W_{fv}; 1-hertz amplitude ratio, 0.10 $(N/cm^2)/(kg/hr)$.

(b) Signal H_3/W_{fv}; 1-hertz amplitude ratio, 0.015 $(N/cm^2)/(kg/hr)$.

(c) Signal $H_{3.5}/P_{fm}$; 1-hertz amplitude ratio, 0.16.

(d) Signal $H_5/\Delta P_{fn}$; 1-hertz amplitude ratio, 0.05.

Figure 8. - Normalized frequency responses of inlet and engine signals for fuel flow disturbances. Engine operating corrected speed, 83.0 percent; compressor pressure ratio, 3.77.

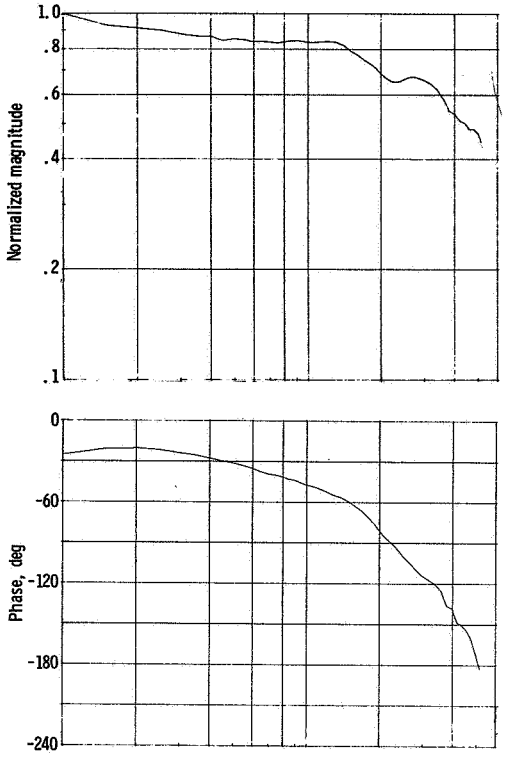

(e) Signal $H_3/\Delta P_{fn}$; 1-hertz amplitude ratio, 0.17.

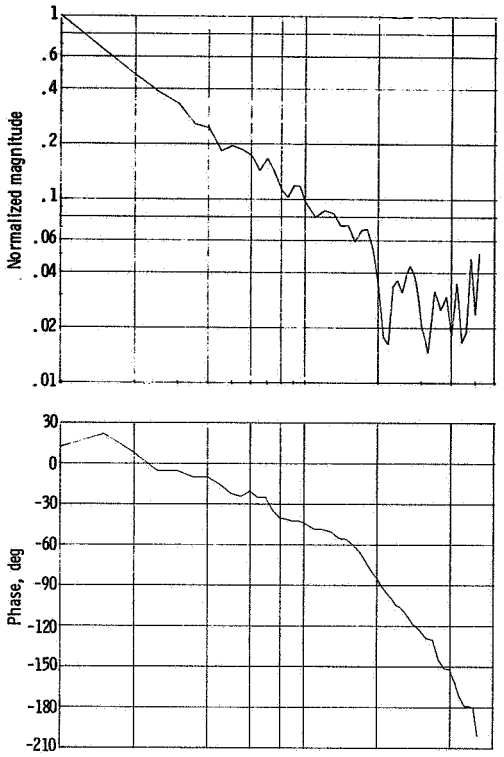

(f) Signal $H_2/\Delta P_{fn}$; 1-hertz amplitude ratio, 0.02.

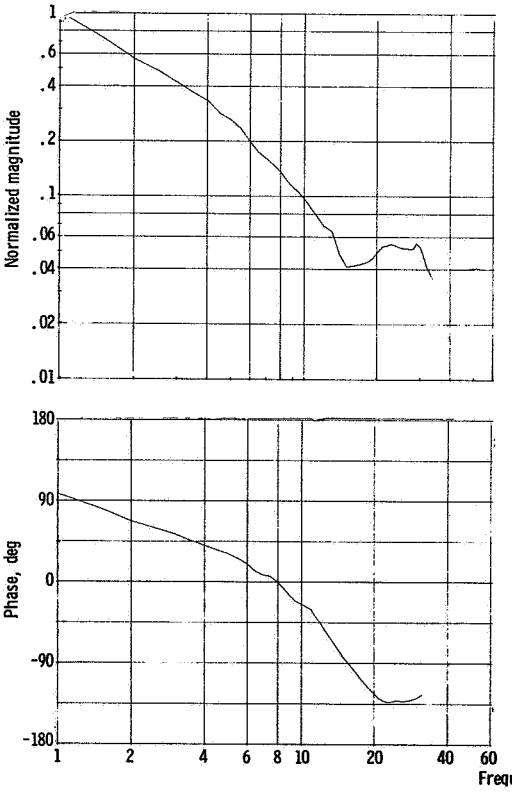

(g) Signal $P_2/\Delta P_{fn}$; 1-hertz amplitude ratio, 0.02.

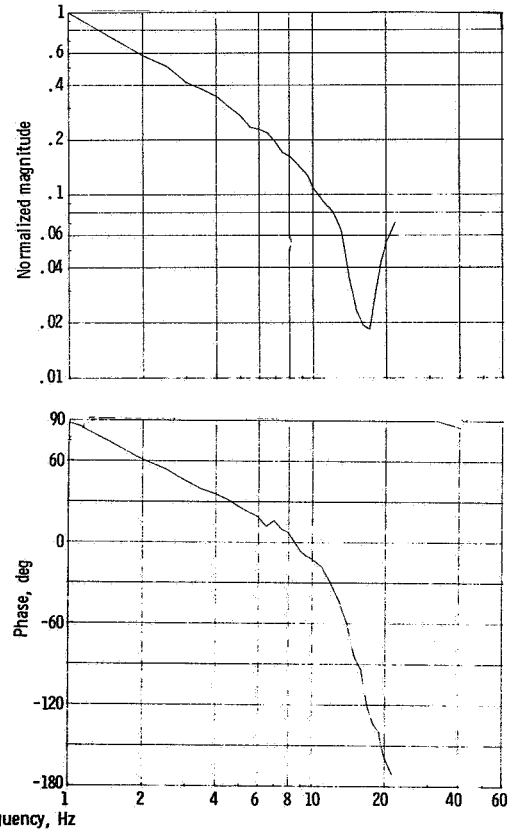

(h) Signal $P_{1.93}/\Delta P_{fn}$; 1-hertz amplitude ratio, 0.01.

Figure 8. - Continued.

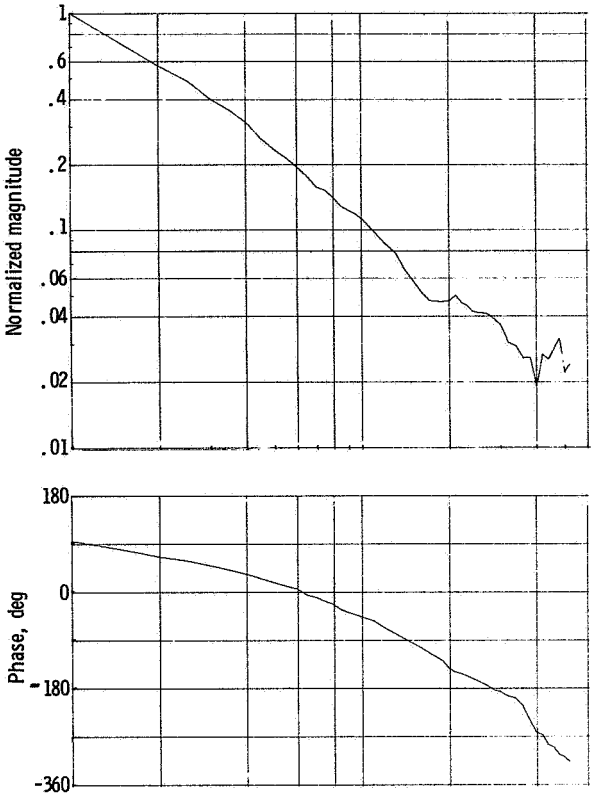

(i) Signal $P_{1.56}/\Delta P_{fn}$; 1-hertz amplitude ratio, 0.11.

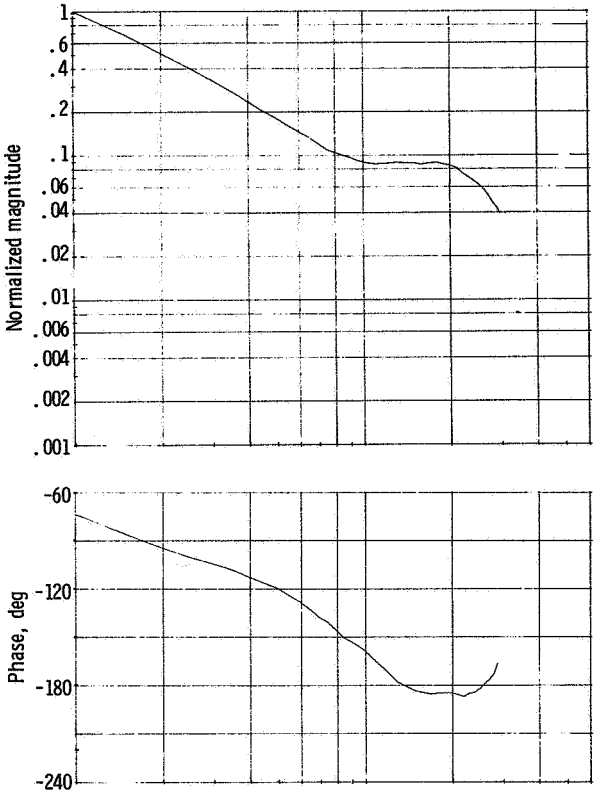

(j) Signal $N/\Delta P_{fn}$; 1-hertz amplitude ratio, 2.4 (rad/sec)/(N/cm^2).

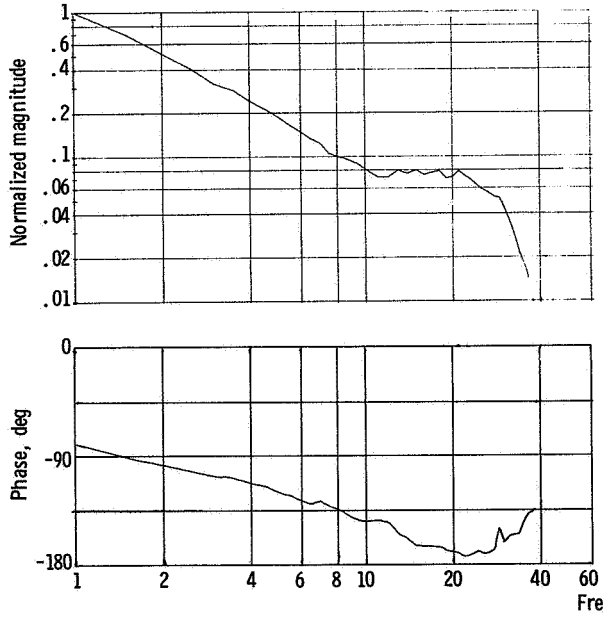

(k) Signal $T_5/\Delta P_{fn}$; 1-hertz amplitude ratio, 2.0 K/(N/cm^2).

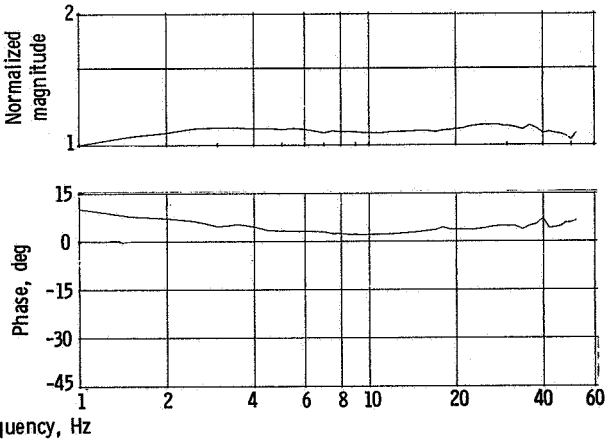

(ℓ) Signal $P_{2.7}/H_3$; 1-hertz amplitude ratio, 0.64.

Figure 8. - Continued.

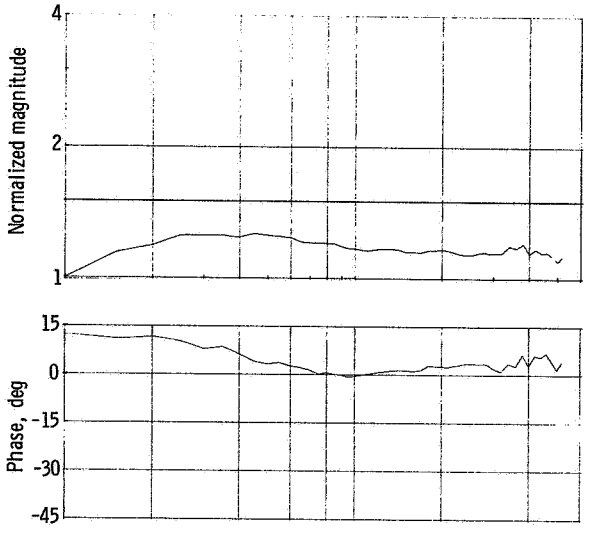

(m) Signal $P_{2.6}/H_3$; 1-hertz amplitude ratio, 0.38.

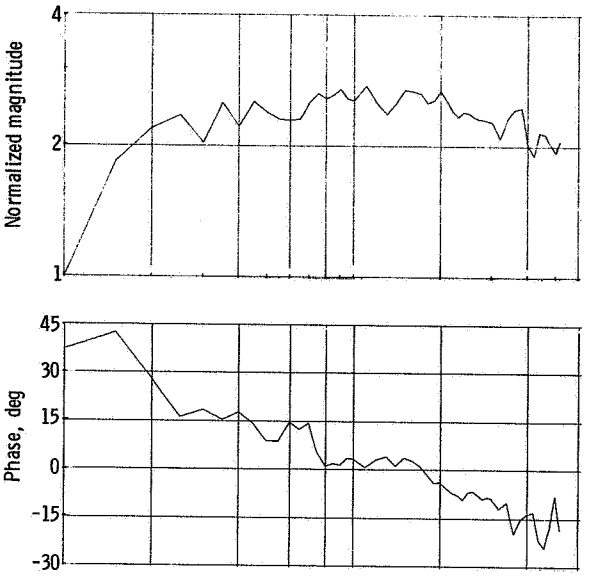

(n) Signal $P_{2.3}/H_3$; 1-hertz amplitude ratio, 0.07.

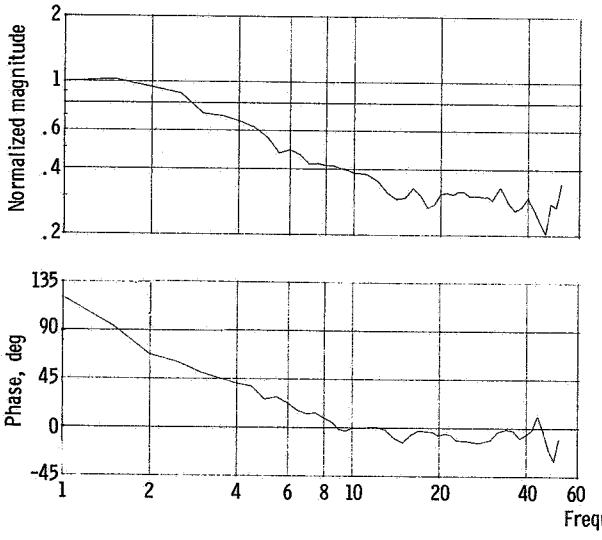

(o) Signal $P_{2.2}/H_3$; 1-hertz amplitude ratio, 0.11.

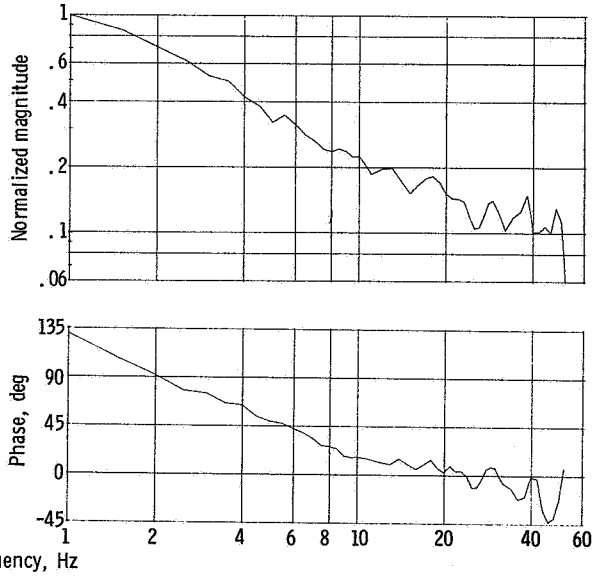

(p) Signal $P_{2.1}/H_3$; 1-hertz amplitude ratio, 0.15.

Figure 8. - Continued.

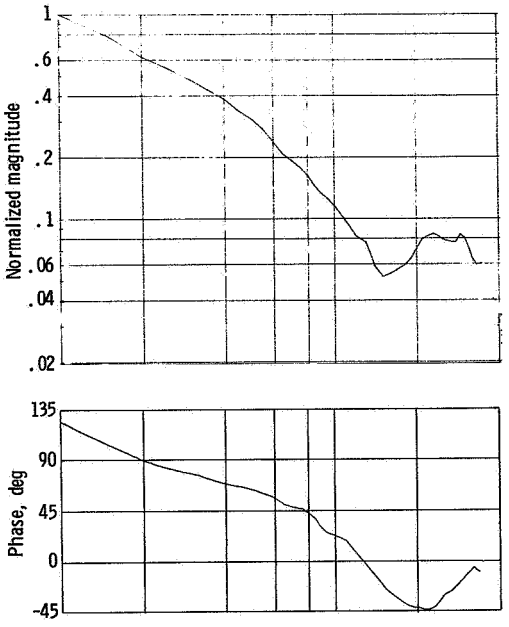

(q) Signal P_2/H_3; 1-hertz amplitude ratio, 0.13.

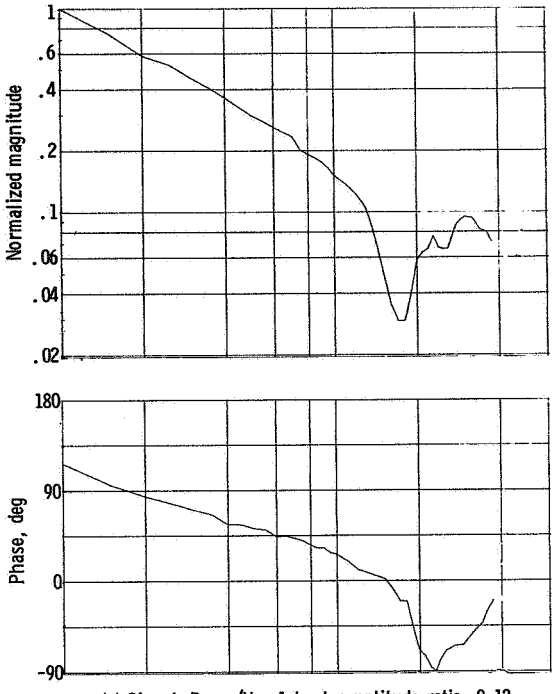

(r) Signal $P_{1.93}/H_3$; 1-hertz amplitude ratio, 0.12.

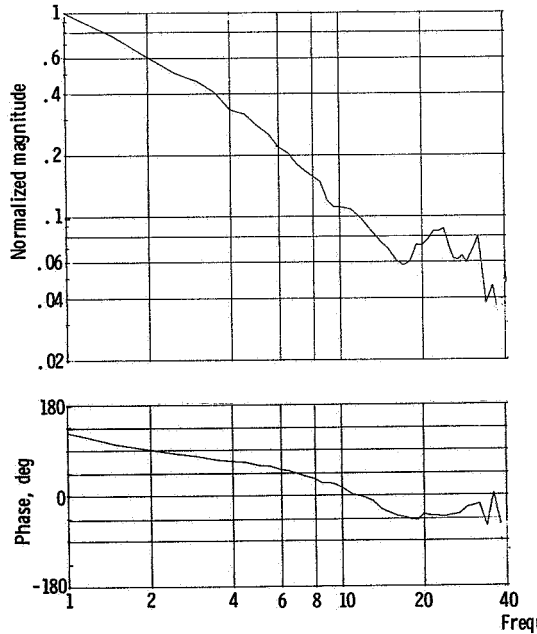

(s) Signal $P_{1.80}/H_3$; 1-hertz amplitude ratio, 0.15.

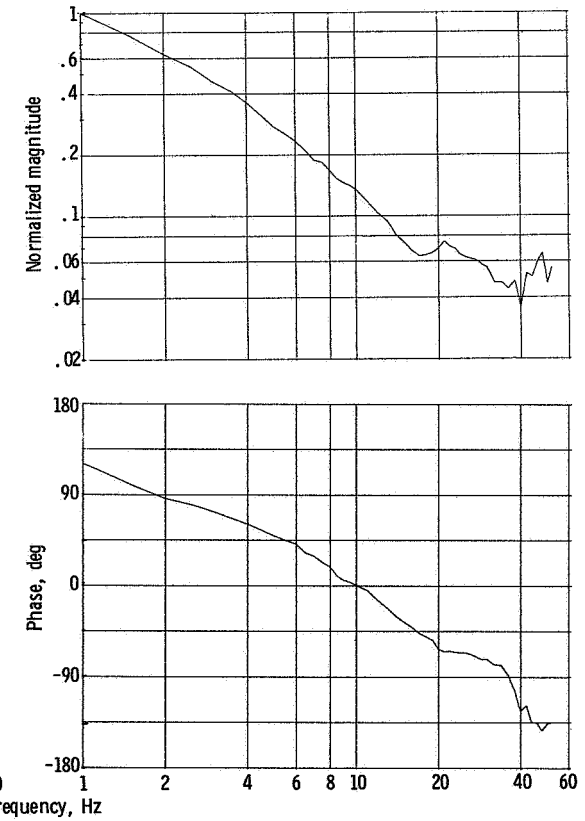

(t) Signal $P_{1.56}/H_3$; 1-hertz amplitude ratio, 0.65.

Figure 8. - Continued.

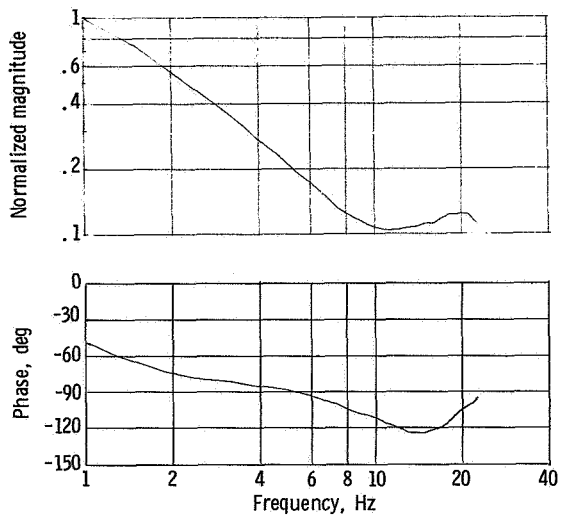

(u) Signal N/H_3; 1-hertz amplitude ratio, 14 (rad/sec)/(N/cm^2).

Figure 8. - Concluded.

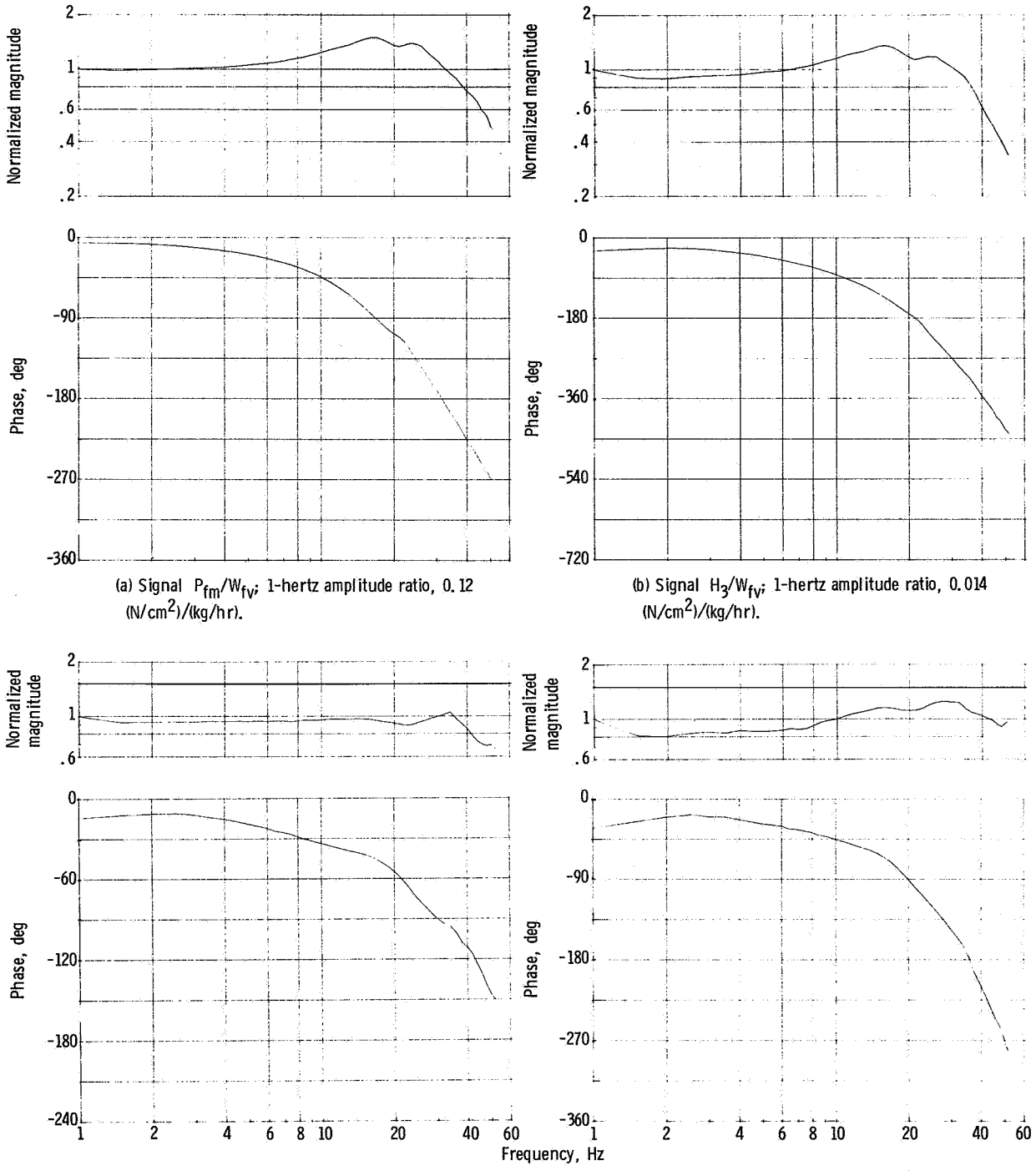

(a) Signal P_{fm}/W_{fv}; 1-hertz amplitude ratio, 0.12 $(N/cm^2)/(kg/hr)$.

(b) Signal H_3/W_{fv}; 1-hertz amplitude ratio, 0.014 $(N/cm^2)/(kg/hr)$.

(c) Signal $H_{3.5}/P_{fm}$; 1-hertz amplitude ratio, 0.15.

(d) Signal $H_5/\Delta P_{fn}$; 1-hertz amplitude ratio, 0.04.

Figure 9. - Normalized frequency responses of inlet and engine signals for fuel flow disturbances. Engine operating corrected speed, 88.2 percent; compressor pressure ratio, 4.63.

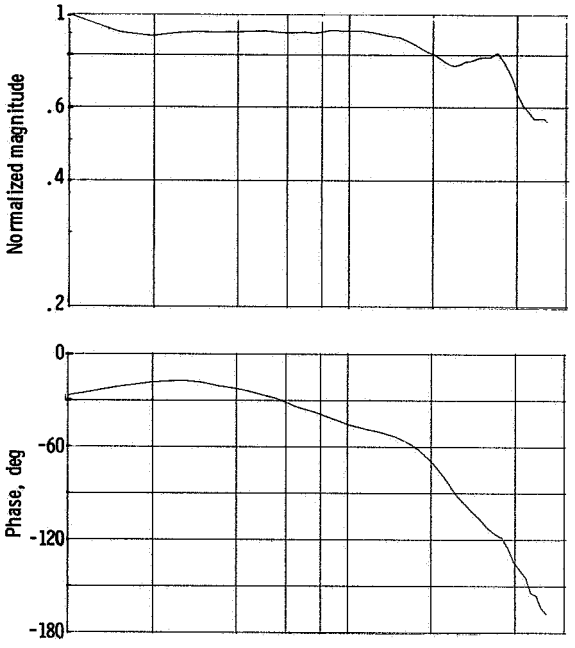

(e) Signal $H_3/\Delta P_{fn}$; 1-hertz amplitude ratio, 0.14.

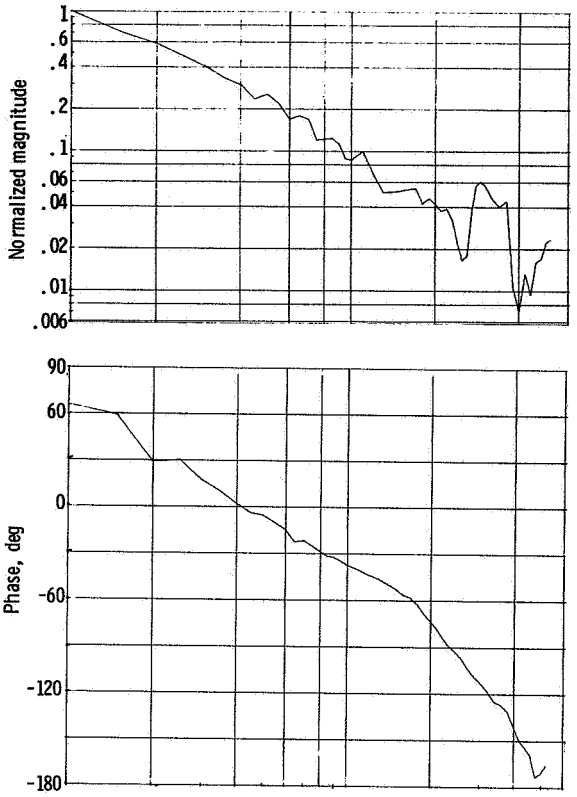

(f) Signal $H_2/\Delta P_{fn}$; 1-hertz amplitude ratio, 0.02.

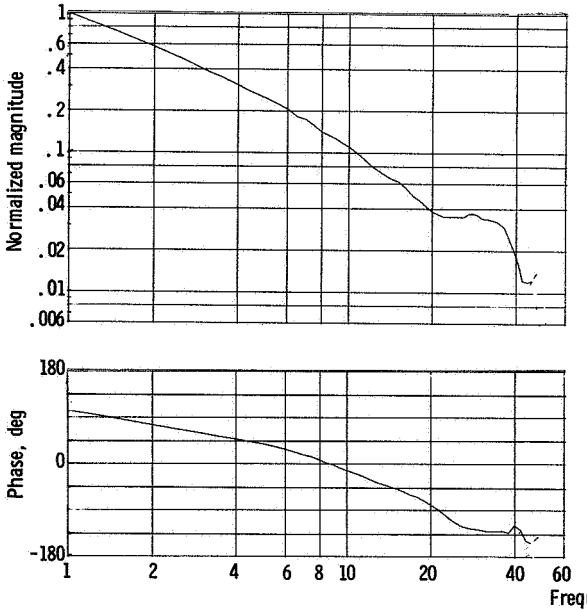

(g) Signal $P_2/\Delta P_{fn}$; 1-hertz amplitude ratio, 0.02.

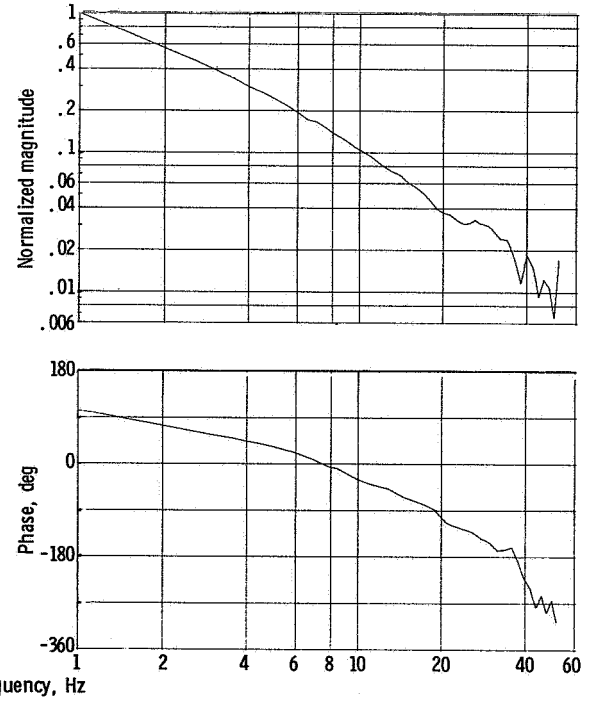

(h) Signal $P_{1.93}/\Delta P_{fn}$; 1-hertz amplitude ratio, 0.02.

Figure 9. - Continued.

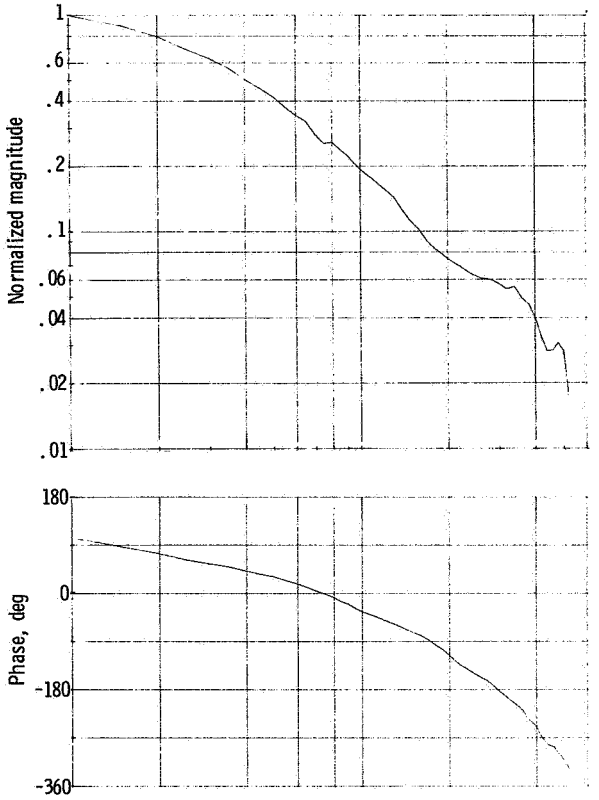

(i) Signal $P_{1.56}/\Delta P_{fn}$; 1-hertz amplitude ratio, 0.07.

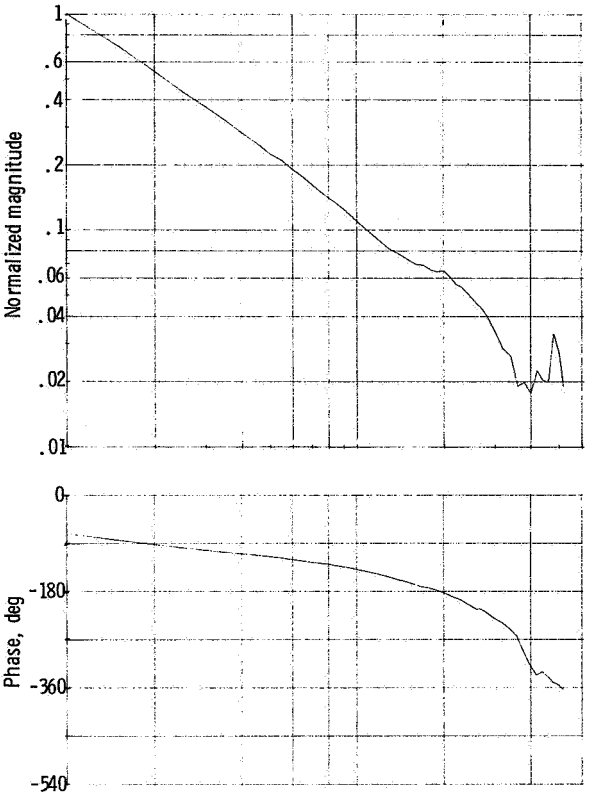

(j) Signal $N/\Delta P_{fn}$; 1-hertz amplitude ratio, 2.3 (rad/sec)/(N/cm^2).

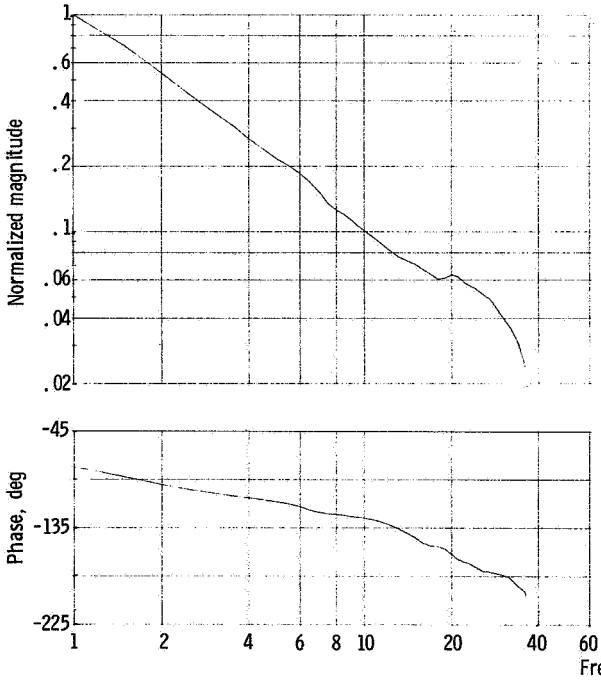

(k) Signal $T_5/\Delta P_{fn}$; 1-hertz amplitude ratio, 1.7 K/(N/cm^2).

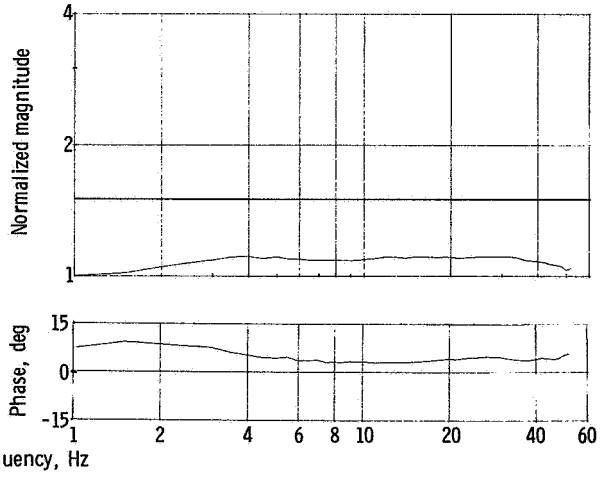

(ℓ) Signal $P_{2.7}/H_3$; 1-hertz amplitude ratio, 0.71.

Figure 9. - Continued.

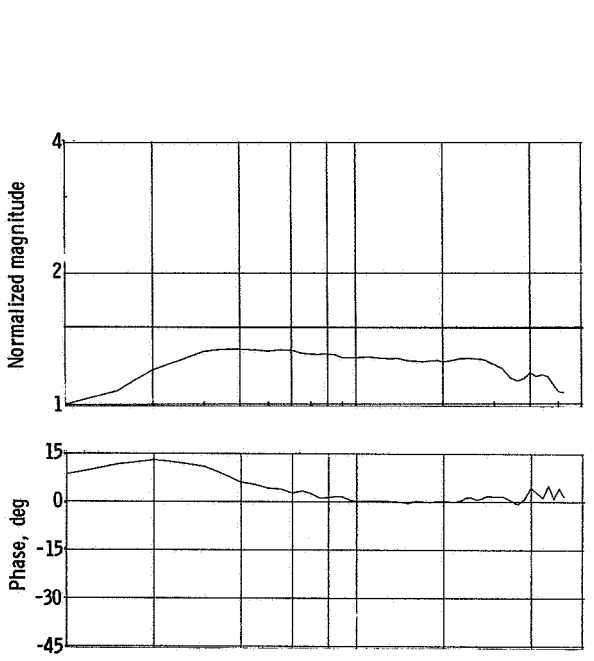

(m) Signal $P_{2.6}/H_3$; 1-hertz amplitude ratio, 0.37.

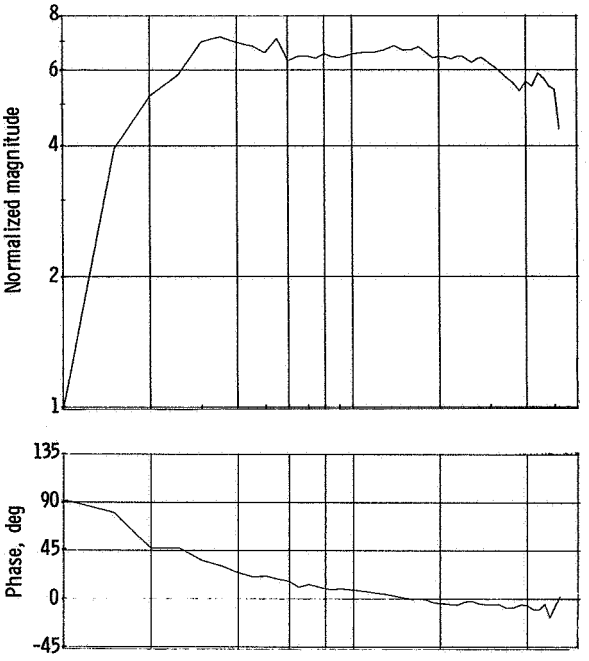

(n) Signal $P_{2.3}/H_3$; 1-hertz amplitude ratio, 0.010.

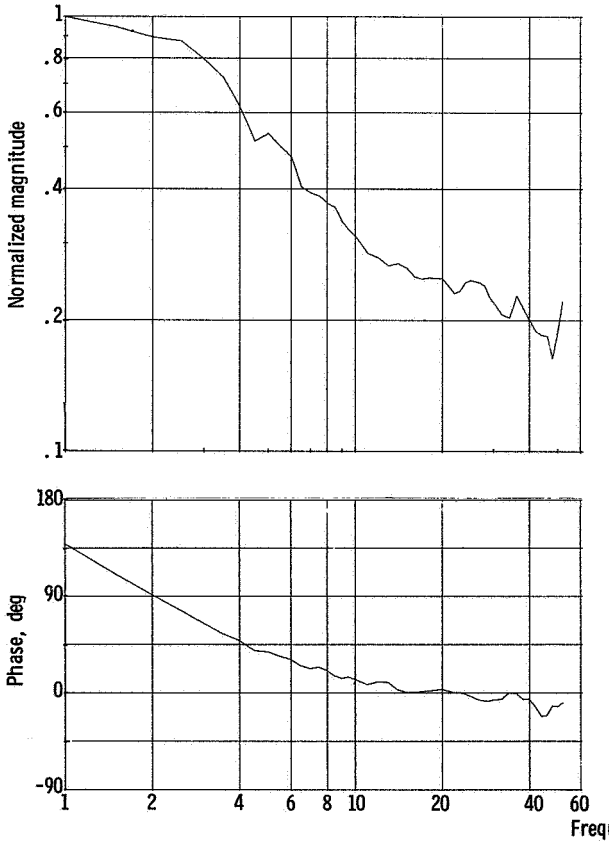

(o) Signal $P_{2.2}/H_3$; 1-hertz amplitude ratio, 0.16.

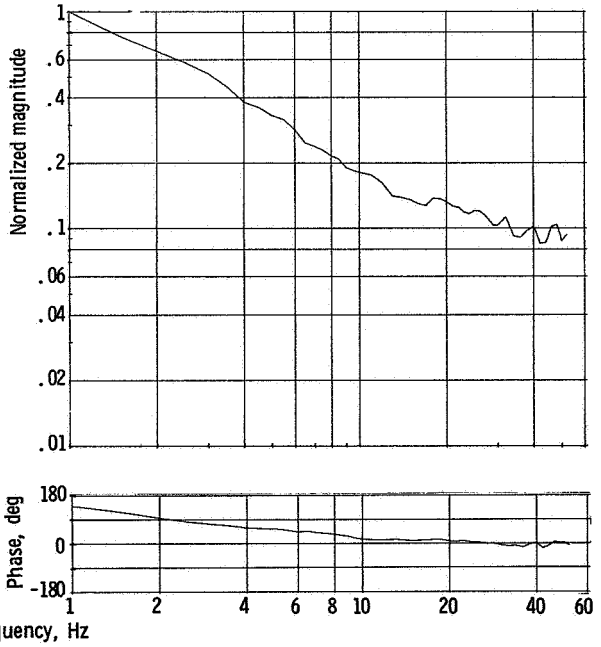

(p) Signal $P_{2.1}/H_3$; 1-hertz amplitude ratio, 0.19.

Figure 9. - Continued.

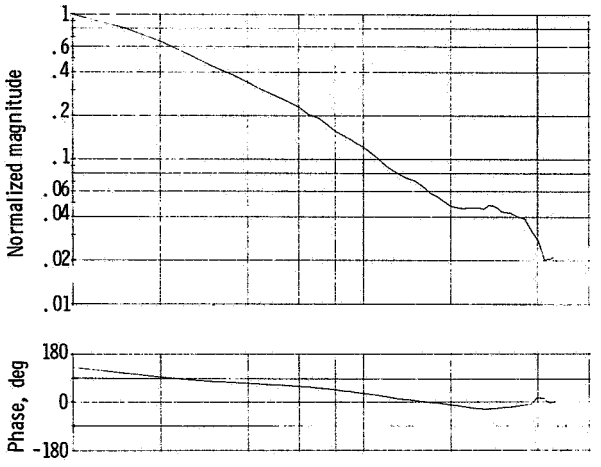

(q) Signal P_2/H_3; 1-hertz amplitude ratio, 0.16.

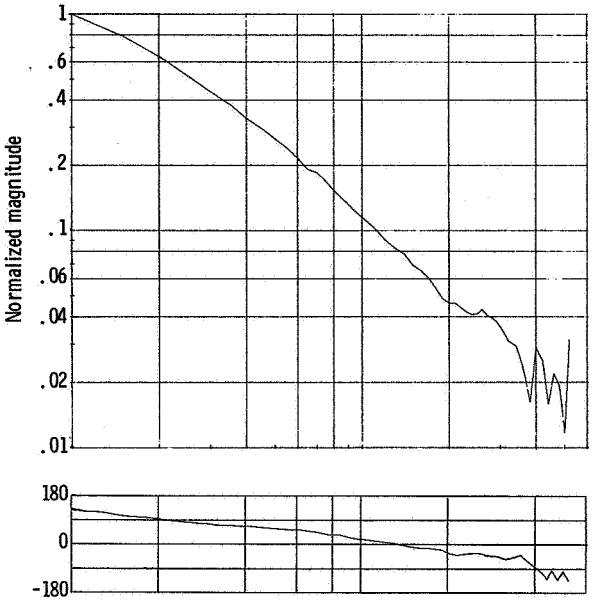

(r) Signal $P_{1.93}/H_3$; 1-hertz amplitude ratio, 0.17.

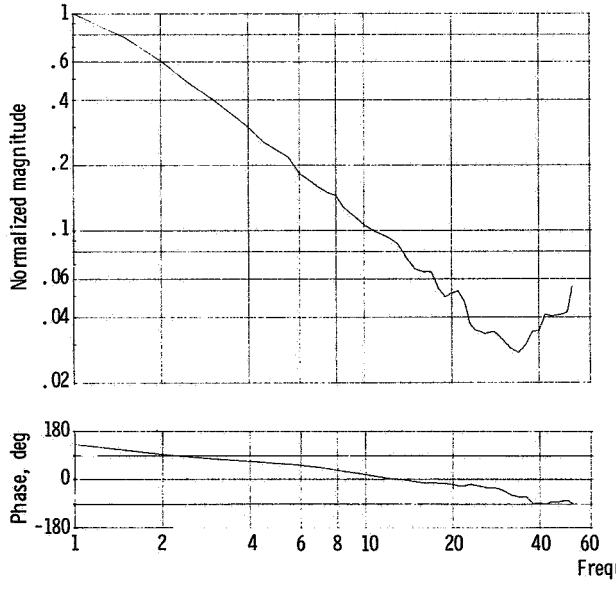

(s) Signal $P_{1.80}/H_3$; 1-hertz amplitude ratio, 0.17.

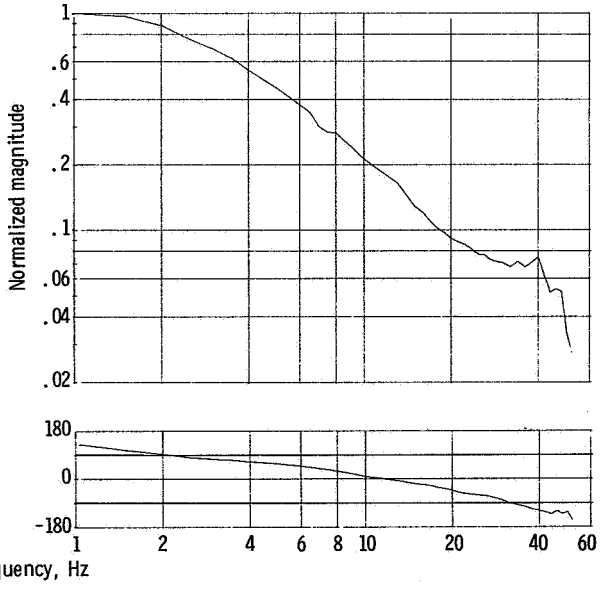

(t) Signal $P_{1.56}/H_3$; 1-hertz amplitude ratio, 0.51.

Figure 9. - Continued.

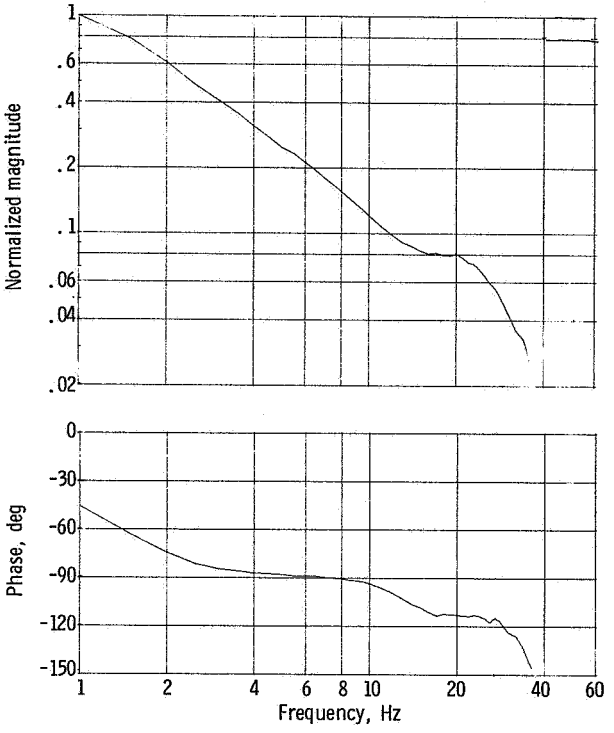

(u) Signal N/H_3; 1-hertz amplitude ratio, 16 (rad/sec)/(N/cm^2).

Figure 9. - Concluded.

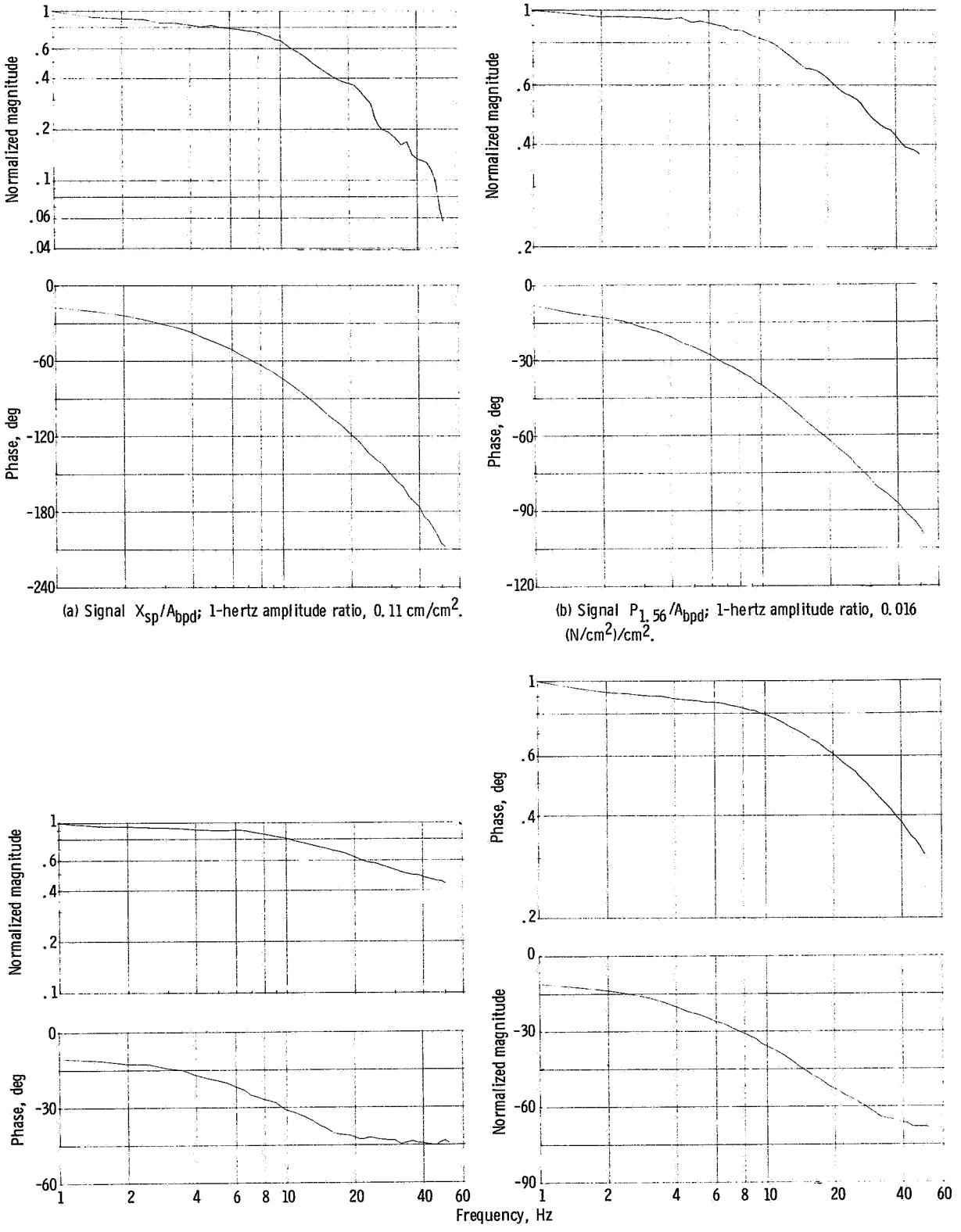

(a) Signal X_{sp}/A_{bpd}; 1-hertz amplitude ratio, 0.11 cm/cm^2.

(b) Signal $P_{1.56}/A_{bpd}$; 1-hertz amplitude ratio, 0.016 (N/cm^2)/cm^2.

(c) Signal $P_{1.93}/A_{bpd}$; 1-hertz amplitude ratio, 0.0032 (N/cm^2)/cm^2.

(d) Signal P_2/A_{bpd}; 1-hertz amplitude ratio, 0.0032 (N/cm^2)/cm^2.

Figure 10. - Normalized frequency responses of inlet and engine signals for overboard bypass airflow disturbances. Engine operating corrected speed, 86.4 percent; compressor pressure ratio, 4.13.

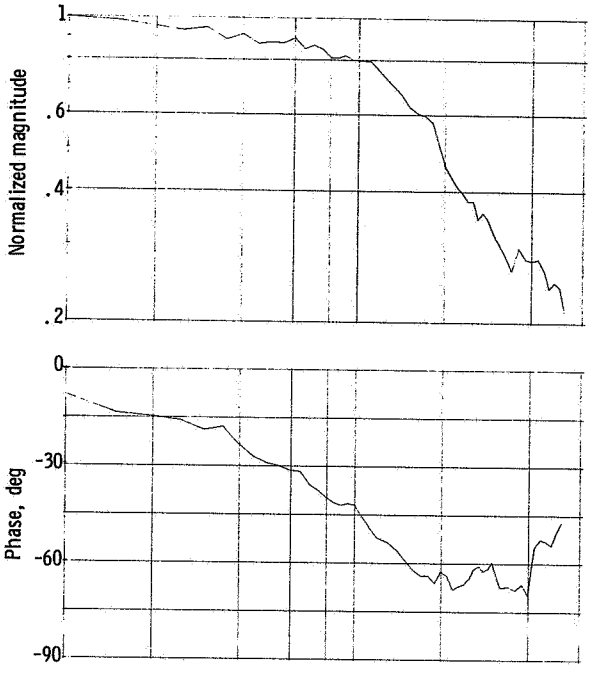

(e) Signal H_2/A_{bpd}; 1-hertz amplitude ratio, 0.0041 $(N/cm^2)/cm^2$.

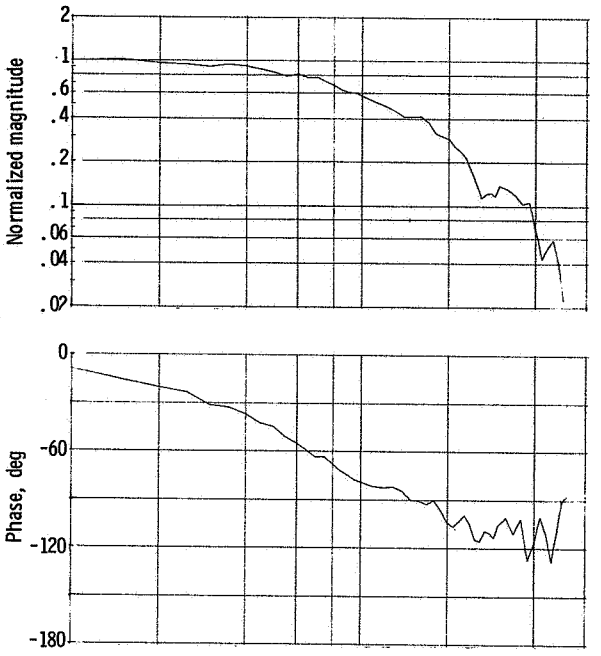

(f) Signal H_3/A_{bpd}; 1-hertz amplitude ratio, 0.040 $(N/cm^2)/cm^2$.

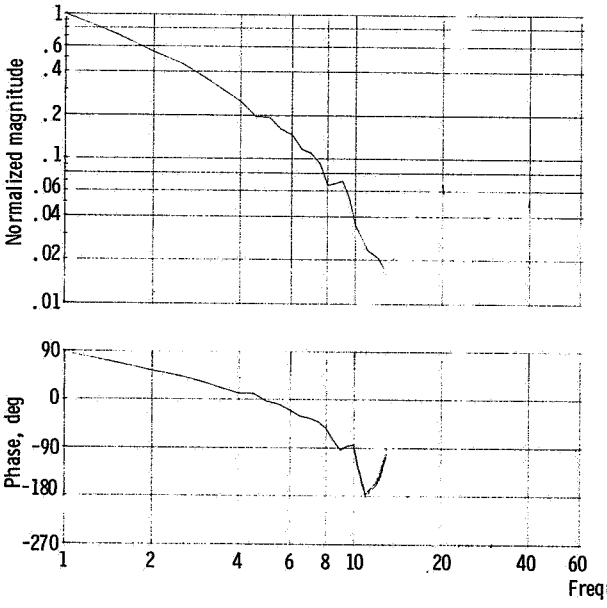

(g) Signal N/A_{bpd}; 1-hertz amplitude ratio, 0.03 $(rad/sec)/cm^2$.

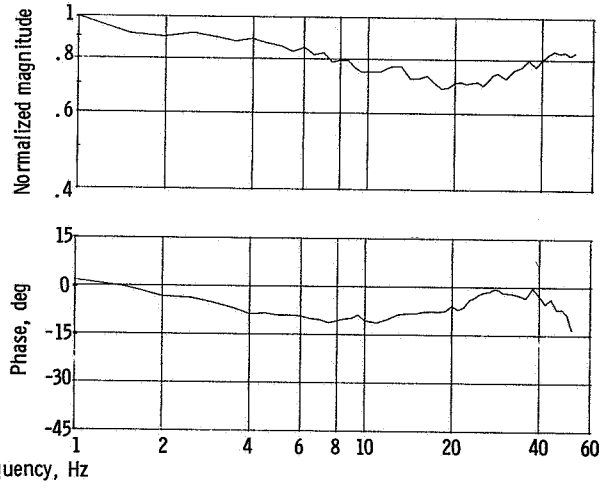

(h) Signal $P_{2.1}/P_2$; 1-hertz amplitude ratio, 1.2.

Figure 10. - Continued.

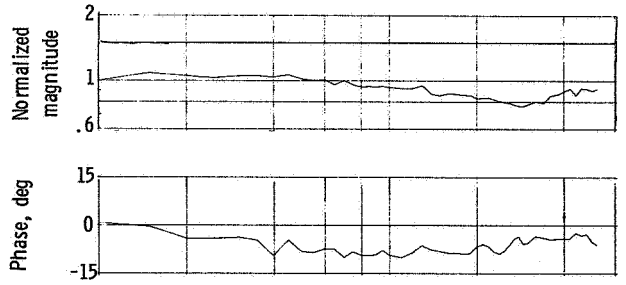

(i) Signal $P_{2.2}/P_2$; 1-hertz amplitude ratio, 1.4.

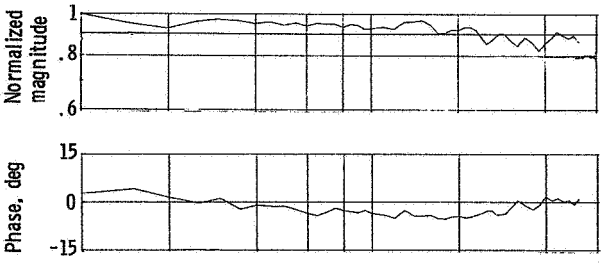

(j) Signal $P_{2.3}/P_2$; 1-hertz amplitude ratio, 2.1.

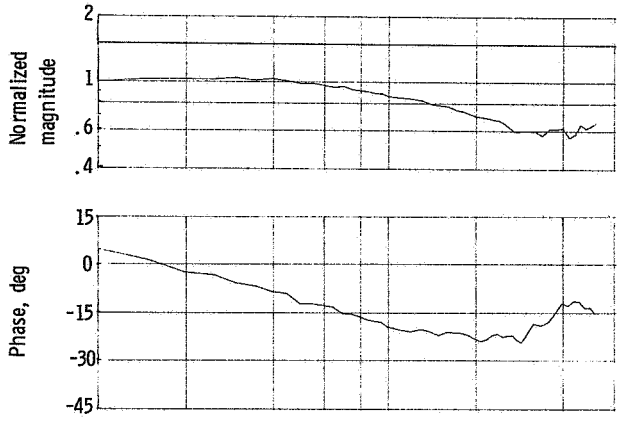

(k) Signal $P_{2.6}/P_2$; 1-hertz amplitude ratio, 3.0.

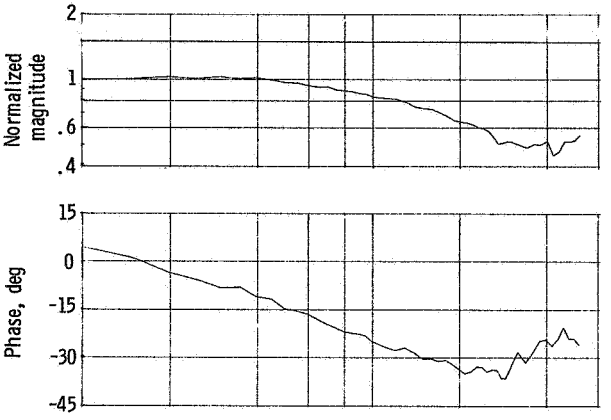

(ℓ) Signal $P_{2.7}/P_2$; 1-hertz amplitude ratio, 3.1.

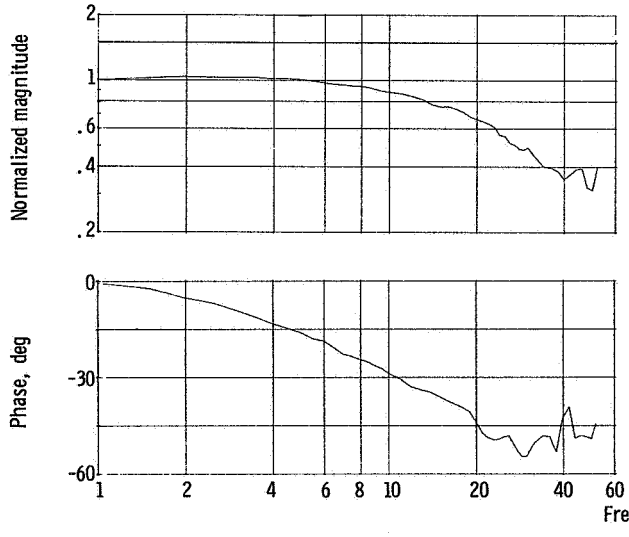

(m) Signal H_3/P_2; 1-hertz amplitude ratio, 3.5.

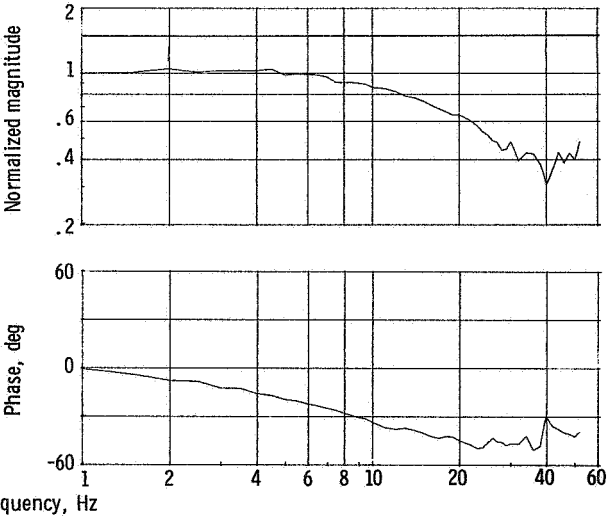

(n) Signal $H_{3.5}/P_2$; 1-hertz amplitude ratio, 3.4.

Figure 10. - Continued.

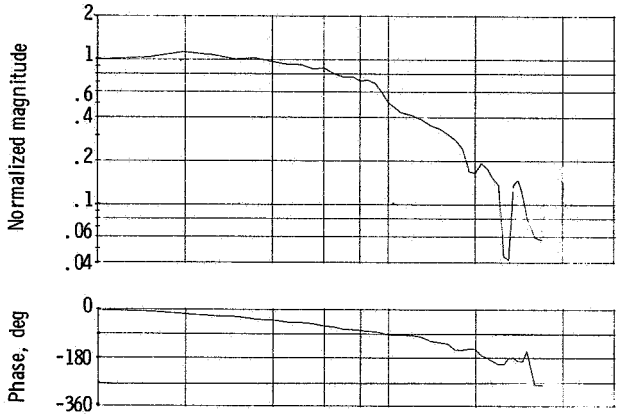

(o) Signal H_5/P_2; 1-hertz amplitude ratio, 1.1.

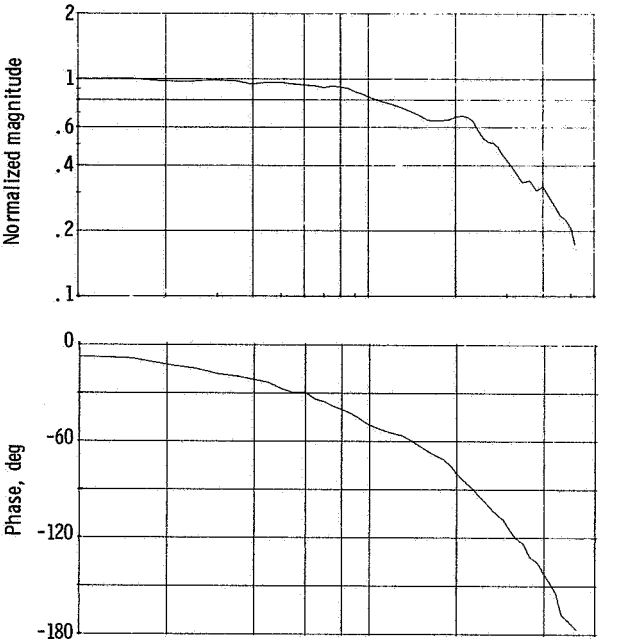

(p) Signal $X_{sp}/P_{1.93}$; 1-hertz amplitude ratio, 31 cm/(N/cm^2).

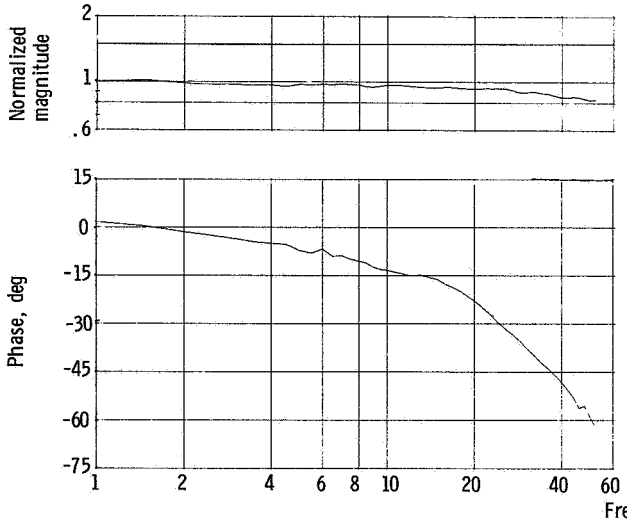

(q) Signal $P_{1.56}/P_{1.93}$; 1-hertz amplitude ratio, 5.0.

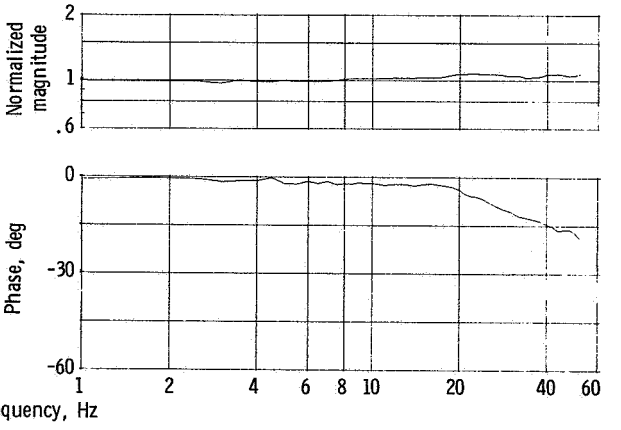

(r) Signal $P_{1.80}/P_{1.93}$; 1-hertz amplitude ratio, 1.4.

Figure 10. - Continued.

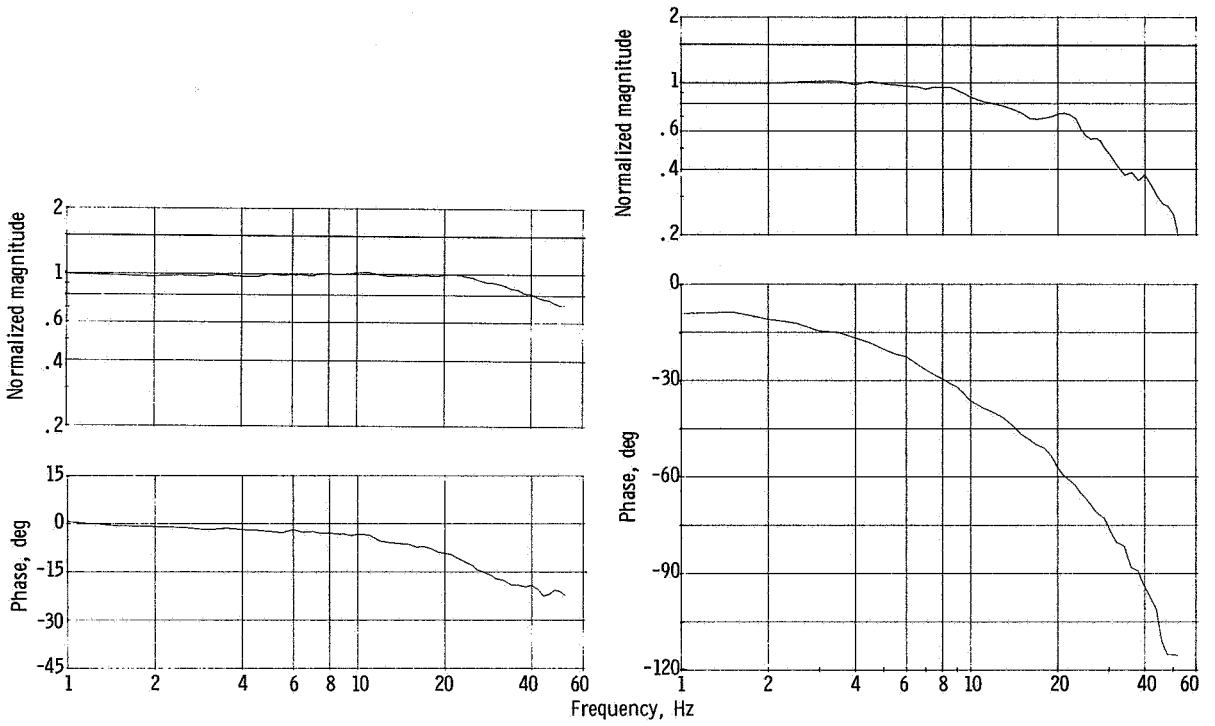

(s) Signal $P_2/P_{1.93}$; 1-hertz amplitude ratio, 1.0.

(t) Signal $X_{sp}/P_{1.56}$; 1-hertz amplitude ratio, 6.3 cm/(N/cm^2).

Figure 10. - Concluded.

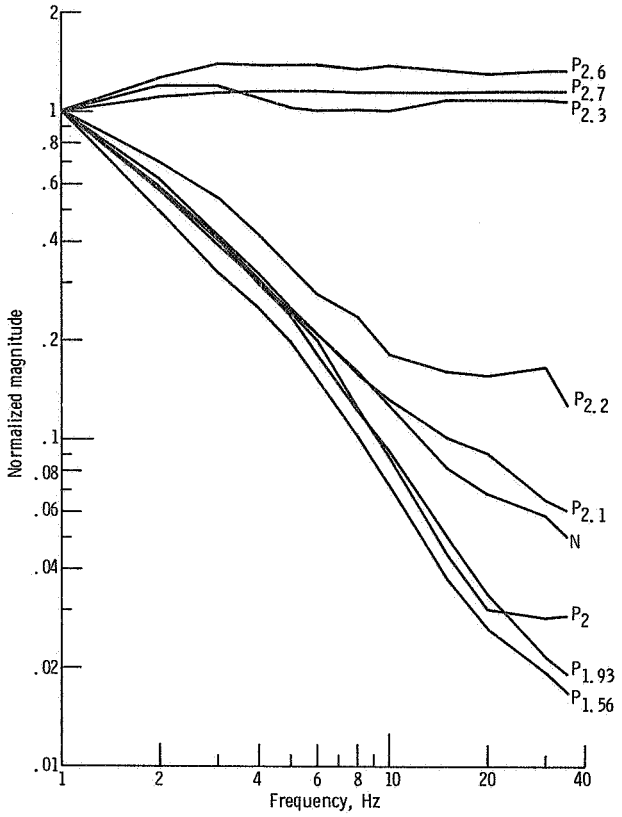

(a) Normalized magnitude response.

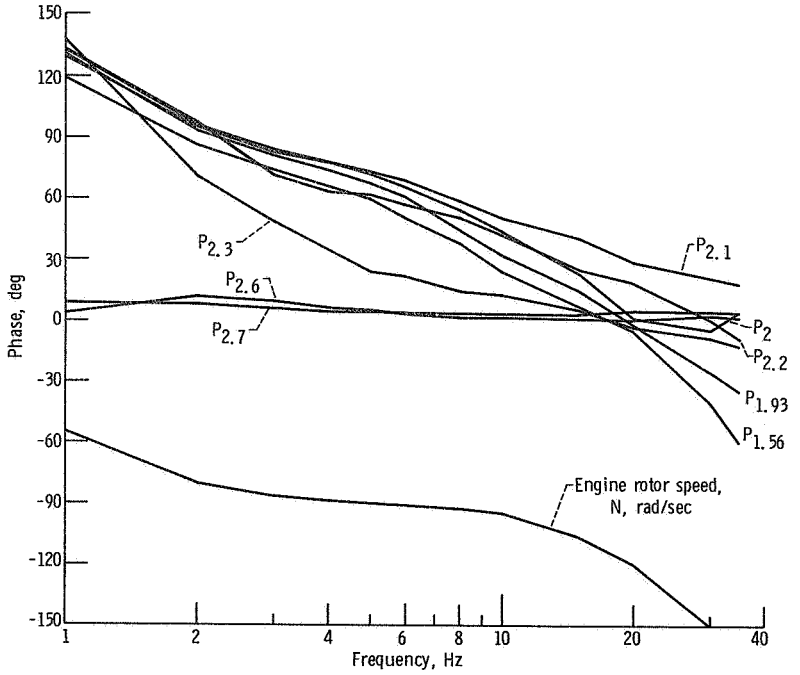

(b) Normalized phase response.

Figure 11. - Composite plot of propulsion system responses normalized to compressor discharge total pressure H_3 for fuel flow disturbances. Engine operating corrected speed 87.8 percent; compressor pressure ratio, 4.17.

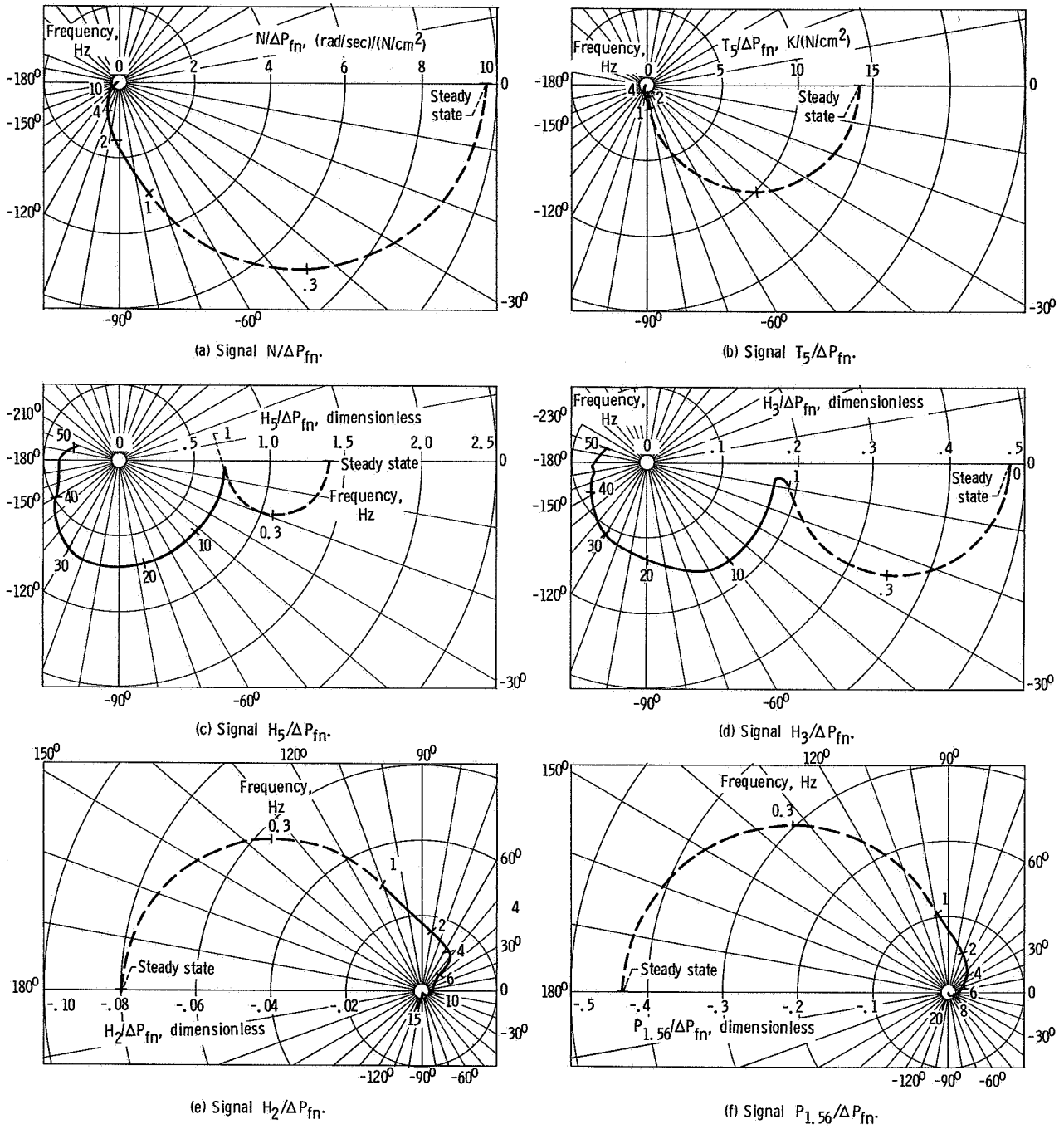

Figure 12. - Response of selected signals with modeled dynamics below 1 hertz for fuel flow disturbance. Engine operating corrected speed, 87.8 percent; pressure ratio, 4.17.

"The aeronautical and space activities of the United States shall be conducted so as to contribute . . . to the expansion of human knowledge of phenomena in the atmosphere and space. The Administration shall provide for the widest practicable and appropriate dissemination of information concerning its activities and the results thereof."

—NATIONAL AERONAUTICS AND SPACE ACT OF 1958

NASA SCIENTIFIC AND TECHNICAL PUBLICATIONS

TECHNICAL REPORTS: Scientific and technical information considered important, complete, and a lasting contribution to existing knowledge.

TECHNICAL NOTES: Information less broad in scope but nevertheless of importance as a contribution to existing knowledge.

TECHNICAL MEMORANDUMS: Information receiving limited distribution because of preliminary data, security classification, or other reasons.

CONTRACTOR REPORTS: Scientific and technical information generated under a NASA contract or grant and considered an important contribution to existing knowledge.

TECHNICAL TRANSLATIONS: Information published in a foreign language considered to merit NASA distribution in English.

SPECIAL PUBLICATIONS: Information derived from or of value to NASA activities. Publications include conference proceedings, monographs, data compilations, handbooks, sourcebooks, and special bibliographies.

TECHNOLOGY UTILIZATION PUBLICATIONS: Information on technology used by NASA that may be of particular interest in commercial and other non-aerospace applications. Publications include Tech Briefs, Technology Utilization Reports and Technology Surveys.

Details on the availability of these publications may be obtained from:

SCIENTIFIC AND TECHNICAL INFORMATION OFFICE

NATIONAL AERONAUTICS AND SPACE ADMINISTRATION

Washington, D.C. 20546